A fully conjugated planar heterocyclic [9]circulene

Stephan K. Pedersen,[†]Kristina Eriksen,[†]Hans Ågren,[‡,&] Boris F. Minaev,[§] Nataliya N. Karaush-Karmazin,[§] Ole Hammerich,[†]Glib V. Baryshnikov,[‡,§]Michael Pittelkow*,[†]

[†]Department of Chemistry, University of Copenhagen, Universitetsparken 5, DK-2100 Copenhagen Ø, Denmark.

[‡]Division of Theoretical Chemistry and Biology, School of Engineering Sciences in Chemistry, Biotechnology and Health, KTH, Royal Institute of Technology, 10691, Stockholm, Sweden.

[&]College of Chemistry and Chemical Enginnering, Henan University, Kaifeng, Henan 475004, P. R. China

[§]Department of Chemistry and Nanomaterials Science, Bohdan Khmelnytsky National University, 18031, Cherkasy, Ukraine

1. Figures Referenced in the Manuscript

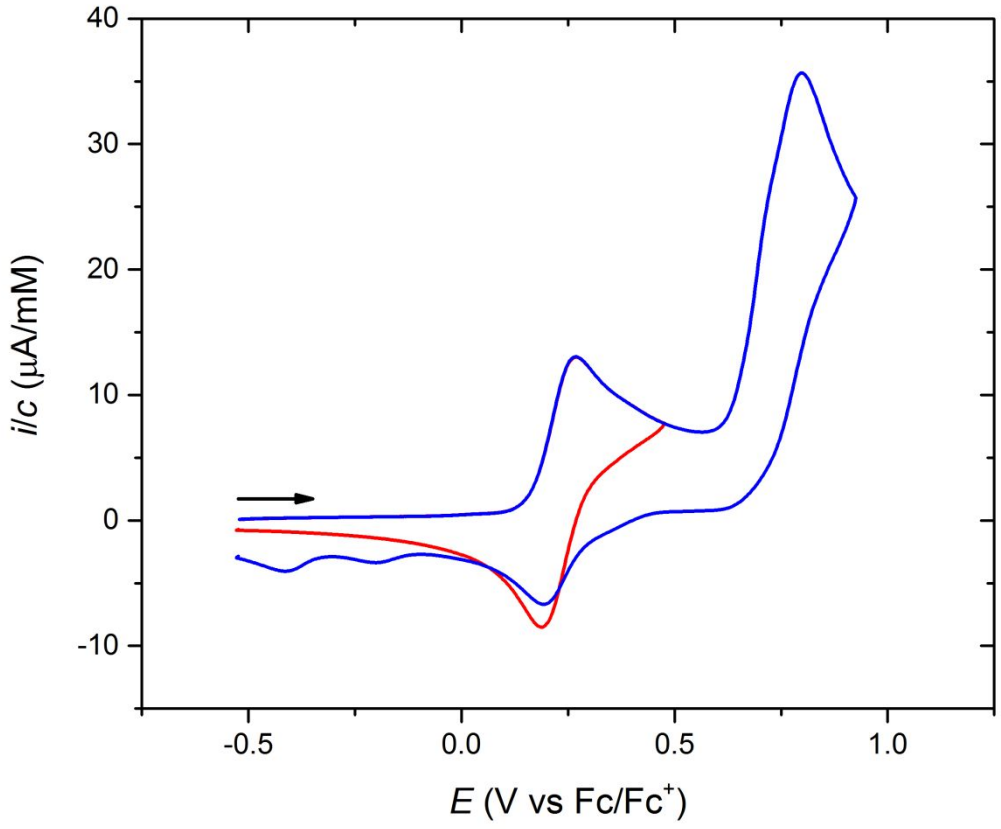

Figure S1: Cyclic voltammograms resulting from the oxidation of **9** (1.61 mM) in CH_2Cl_2 (0.1 M Bu_4NPF_6) at a glassy carbon working electrode (d = 3 mm). The voltage sweep rate was 0.1 V s^{-1}.

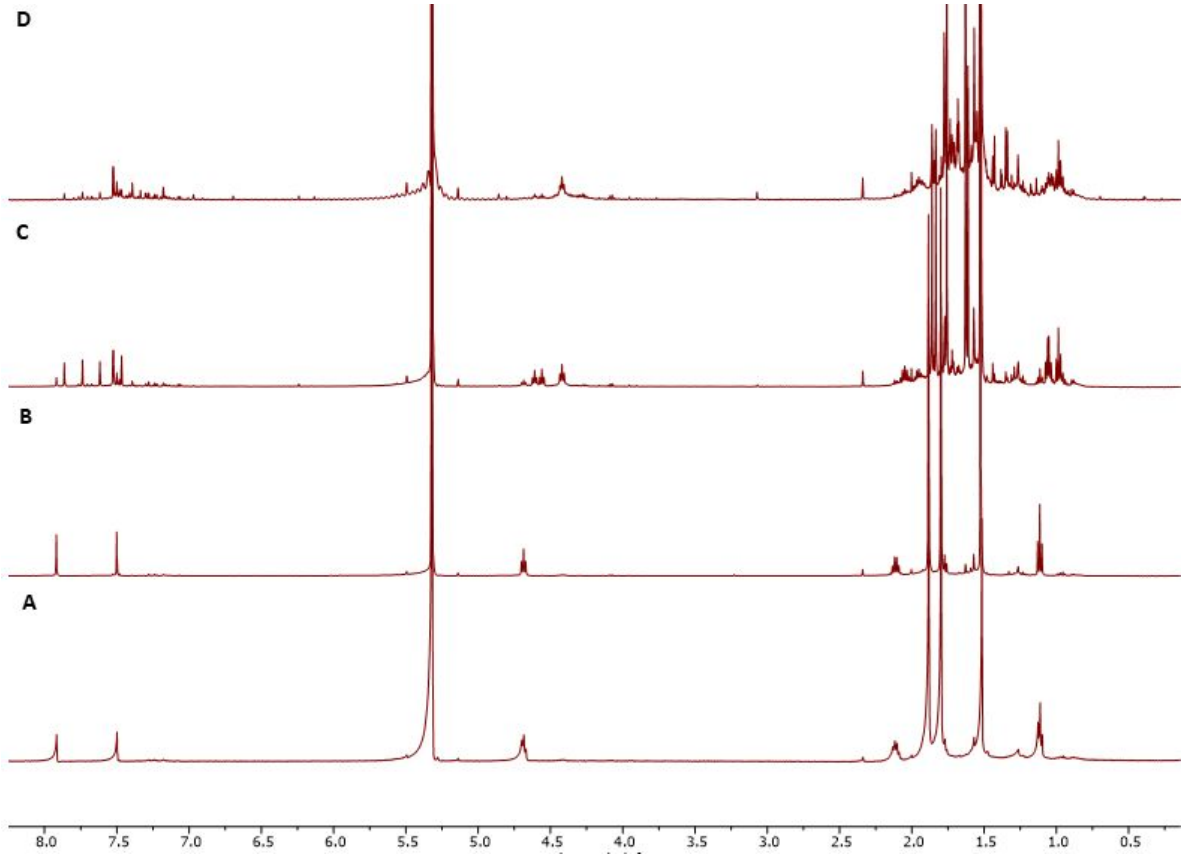

Figure S2: Decomposition of **9** under ambient light conditions, sample is 0.02 M in CD_2Cl_2. **A** is a freshly prepared sample. **B** has been shielded from light for 48 hours. **C** has been exposed to ambient light for 1.5 h. **D** has been exposed to ambient light for 24 h.

To identify the initial decomposition products of **9**, when exposed to ambient light in non/degassed CD_2Cl_2, the crude mixture was analyzed using MALDI-TOF(+) (Figure S3). After 1.0 hour the masses of photooxygenation products **9-OH** and **9-(OH)$_2$** was observed as part of the decomposition of **9**.

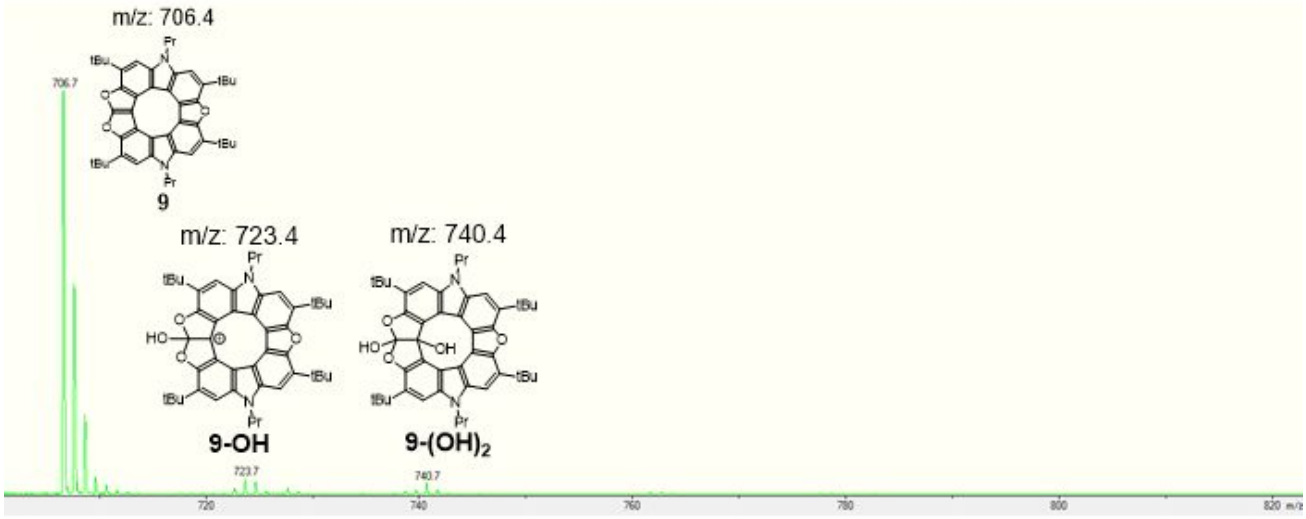

Figure S3: MALDI-TOF(+) of a 0.02 M sample of 9, in CD_2Cl_2 kept under ambient light conditions for 1.0 hours.

Closer inspection of pertinent regions of the ^{1}H-NMR (8.0 – 7.0 ppm and 4.9 – 4.3 ppm) of a similar sample after 1.5 hour of ambient light exposure, i.e. from Figure S2C, three major products are arguably observed in the ratio 1.00:1.10:1.42 (circle:triangle:square, respectively, Figure S4). This can be assigned to what is expected from **9-OH** and the set of diastereoisomers for **9-(OH)$_2$**. Numerous attempts to isolate any of the proposed structures, proved futile due to complete decomposition to a variety of unknown products during purification.

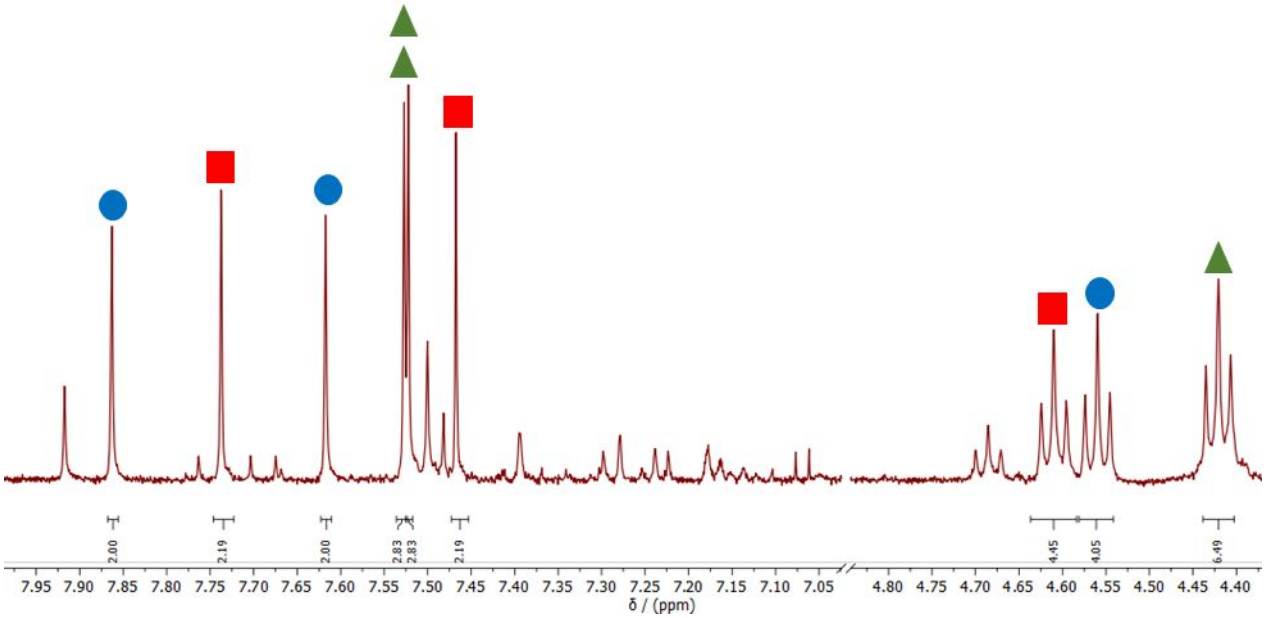

Figure S4: Close up of the ^{1}H-NMR spectra shown in Figure S2C, and the assignment of the formation of three major product.

2. Computational Details

2.1. Method

The equilibrium structures of the molecules **9** and **10** in the ground singlet state have been optimized using the density functional theory (DFT) method with the hybrid B3LYP functional [1–2] and the Pople's split-valence double-zeta 6-31G(d) basis set with additional polarization d-functions. [3]

The obtained optimized geometry of these molecules was then usedfor the calculation of vertical singlet-singlet electronic transition spectra within the framework of time-dependent densityfunctional theory (TD DFT) in the vacuum approximation and by using the polarizable continuum model of solvation (PCM) taking the DCM (ε= 2.37) as a model solvent. [4] The calculated electronic absorption spectra of the molecules **9** and **10** were created by using the SWizard software [5] (band half-width 3000 cm-1, Gaussian distribution).

The nucleus-independent chemical shifts (NICS) [6] at the ring centers (denoted NICS(0)) were calculated at the B3LYP/6-311++(d,p) [7, 8] level of theory with the gauge-independent atomic orbital (GIAO) approximation [9] in order to evaluate the local magnetic properties of the selected molecules. Negative values of the NICS(0) indexes indicatethe existence of induced diatropic ring currents, *i.e.*, aromaticity; positive values of the NICS(0) indexes correspond to paratropic ring currents, *i.e.*, antiaromaticity.[10] In the cases when the absolute values of NICS indexes are close to zero, the ring is non-aromatic. [11]

In order to probe the charge-transport properties of the studied heterocirculenes, the incoherent hopping model was used. [12–17] According to this model, charge carriers (holes and electrons) can transfer between adjacent molecules in crystals. The rate of charge transfer (k) can be expressed by the Marcus-Hush equation [18–21]

$$k = \frac{4\pi^2}{h}\frac{1}{\sqrt{4\pi\lambda k_B T}}V^2 \exp\left(-\frac{\lambda}{4k_B T}\right) \quad \text{(S1)}$$

where V is the transfer integral between two adjacent molecules, λ is the reorganization energy, h and k_B are the Planck and Boltzmann constants, and T is the temperature (298.15 K for our calculations). Accordingly to the above equation (1), a high rate of charge hopping k is attained when the transfer integral (V) between two molecules is high, and the monomers have low reorganization energy (λ). The mobility (μ) of the charge carriers can be calculated using the Nernst-Einstein relation

$$\mu = \frac{e}{k_B T}D \quad \text{(S2)}$$

where D is the diffusion coefficient. The diffusion coefficient can be approximately calculated as a sum of all possible charge carrier hops to the i-th neighbor with the d_i distance to i neighbor

$$D = \frac{1}{2n}\sum_i d_i^2 k_i P_i \quad \text{(S3)}$$

where n is the dimensionality of the crystal (here n = 3), and P_i is the relative probability for charge carrier to *i*-th neighbor normalized over the total hopping rate ($\sum_i k_i$).

The reorganization energies for hole (λ_+) and electron (λ_-) charge carriers are calculated as the sum of geometrical relaxation energies upon going from the neutral-state geometry to the charged-state one and vice versa [22–25]

$$\lambda_{+/-} = (E^*_{+/-} - E_{+/-}) + (E^{**}_{+/-} - E_0) \quad \text{(S4)}$$

where E_0 is the optimized ground state energy of the neutral molecule, $E_{+/-}$ is the optimized energy of the cationic/anionic molecule, $E^{**}_{+/-}$ is energy of the neutral molecule at the cationic/anionic geometry, and $E^*_{+/-}$ is energy of the cationic/anionic molecule at the neutral-state geometry.

Starting from the S_1 optimized excited state geometries of circulenes **8**, **9** and **10** the spin-orbit coupling (SOC) effects were treated as a perturbation based on the scalar relativistic (SR) orbitals after SCF and TDDFT calculations (pSOC-TDDFT); [26] B3LYP functional, Slater-type DZP all-electron basis set [27] and COSMO continuum solvation model (hexane as a solvent) [28] were used for these calculations. The SOC matrix elements, $\langle S_1 | \hat{H}_{SO} | T_j \rangle$ (j=1,2,3…; $E(S_1) > E(T_j)$) were calculated as root mean squares, *i.e.* as square root of the sum of squares of spin-orbit coupling matrix elements of all triplet state sublevels (m=0,±1) of the uncoupled states: [29]

$$\langle S_i | \hat{\mathbf{H}}_{\mathbf{SO}} | T_j \rangle = \sqrt{\sum_{m=0,\pm1} \langle S_i | \hat{\mathbf{H}}_{\mathbf{SO}} | T_j^m \rangle^2}\,. \quad \text{(S5)}$$

The spin-orbit coupling operator $\hat{\mathbf{H}}_{\mathbf{SO}}$ was considered in our calculations within the zeroth-order regular approximation (ZORA) [30, 31] in accordance with the following expression:

$$\hat{\mathbf{H}}_{\mathbf{SO}} = \frac{c^2}{\left(2c^2 - V\right)^2}\boldsymbol{\sigma}\left(\nabla V \cdot \mathbf{p}\right), \quad \text{(S6)}$$

where **σ**– Pauli spin matrix vector, **p** – the linear momentum operator; c – speed of light, V– Kohn−Sham potential. The fluorescence rate constants (k_r) were estimated according to the following relationship (expressed in atomic units): [32, 33]

$$k_r = \frac{1}{\tau} = \frac{2\left(\Delta E^2\right) f}{c^3}, \quad \text{(S7)}$$

where τ is a radiative life of the S_1 state, ΔE and f – the energy and oscillator strength of the corresponding singlet-singlet or singlet-triplet transitions with accounting of SOC perturbations.

The rate constants of intersystem crossing (ISC) between the S_1 and T_j states $E(S_1) > E(T_j)$ were estimated using the Plotnikov's empirical approximation: [34]

$$k_{S_1 \to T_j} = 10^{10} \left\langle S_1 \left| \hat{\mathbf{H}}_{\mathbf{so}} \right| T_j \right\rangle^2 F_{0m}, \quad \text{(S8)}$$

where Franck-Condon factors (F_{0m}) were approximated using the formula:

$$F_{0m} = \sum_n \prod_\nu \frac{e^{-y} y^{n_\nu}}{n_\nu!}. \quad \text{(S9)}$$

In Eq. (9) the Huang–Rhys factor y was assumed to be equal to 0.3 and only one average promotive mode ω_ν = 1400 cm^{-1} was used when considering $n_\nu = \Delta E(S_1\text{-}T_j)/\omega_\nu$. Such a single-mode approximation was considered efficient and accurate enough for the organic dyes and hetero[8]circulenes. [35–38]

The charge carriers mobilityand pSOC-TDDFT calculations were carried out using the ADF2018 package [39] while the rest of calculations were performed using Gaussian16 software. [40]

The diazatrioxa[9]circulene (**9**) was shown to be planar in the solid state and our DFT calculations also confirm planar structure of diazatrioxa[9]circulene (**9**) free molecule in gas phase and in CH_2Cl_2. The optimized geometry of the free molecule calculated at the B3LYP/6-31(d) level of theory can be easily constructed by using Cartesian coordinates (Table S3 and Fig. S5). Such planar structure of **9** can be, in principle, explained by the structural Wynberg-Dopper model which determines the shape of circulene molecules as the sum of the sector angles ($\sum_{sect}$) of the individual rings included in the outer circulene macrocycle (J. Org. Chem., 1975, 40, 1957–1966). According to this model, the circulene molecule is planar if the sum of all sector angles is equal to 360° or close to this value. In accordance with X-ray data it is accepted in the literature that the sectorial angle of free benzene molecule is 60°, furan – 32° and pyrrole – 35°. For diazatrioxa[9]circulene the sectors of benzene, furan and pyrrole rings are presented in Fig. 1. It is interesting to note that the sectors of benzene rings in diazatrioxa[9]circulene molecule decrease significantly up to 38° and 40° for rings B and D, respectively, which is much less than that (around 60°) in coronene, diazadioxa[8]circulene etc. (J. Org. Chem., 1975, 40, 1957–1966; Synlett., 2015, 27, 498–525). The sectors for furan and pyrrole in **9** are slightly larger than those sectors of furan and pyrrole and vary in the range ≈39.5°–43°. Therefore, the sum of sectorial angles of **9** is 360° indicating perfectly planar structure of diazatrioxa[9]circulene. The same phenomenon of planarity and almost unstrained structure upon conjugation of nine thiophene rings (individual sector is 45° that gives in sum 9x45°=405°>360°) was previously reported for octathia[8]circulene (Angew. Chem. Int. Ed., 2006, 45, 7367–7370, New J. Chem., 2019, 43, 12178–12190). The origin of such planarization effect for octathia[8]circulene and diazatrioxa[9]circulene 9 most probably comes from aromatic "stabilization" that overcomes the strain effect upon addition of one five-membered "extra" ring (furan in case of diazatrioxa[9]circulene and thiophene in case of octathia[8]circulene). One can expect that addition of one extra benzene ring with larger sectorial angle or inclusion of several extra rings into the planar diazadioxa[8]circulene will lead to saddle-shaped structures because of in that case aromatic stabilization within outer perimeter should not able to overcome the strain effect, so diazatrioxa[9]circulene is most likely the biggest possible planar heterocirculene.

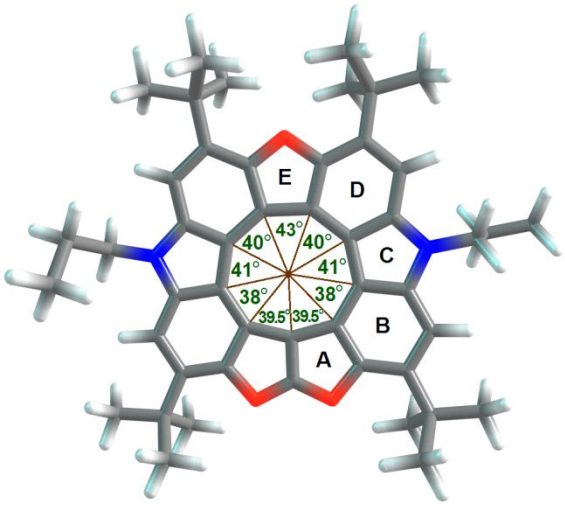

The sectors of furans (A, E), pyrrole (C) and benzene (B, D) rings in diazatrioxa[9]circulene.

2.2. Optimized Structures

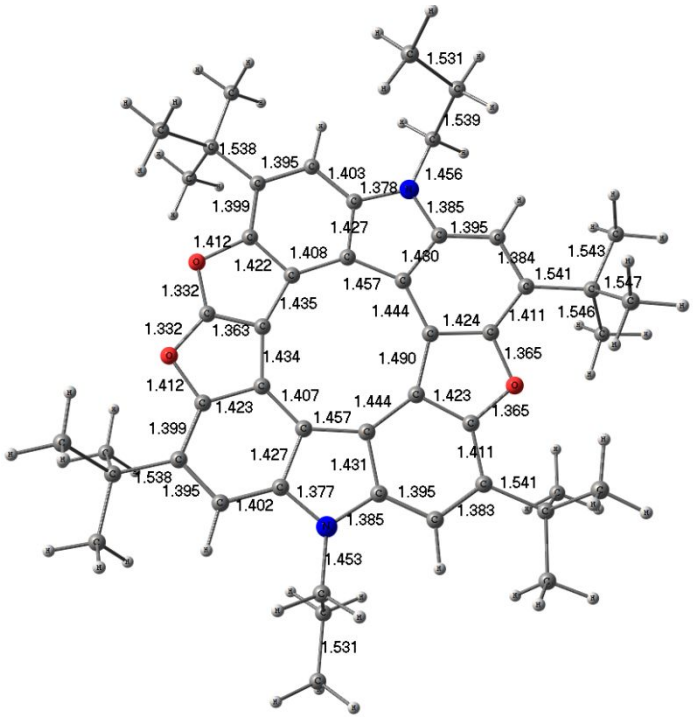

Figure S5: The optimized structure of compound **9** in the ground singlet state calculated at the B3LYP/6-31(d) level of theory.

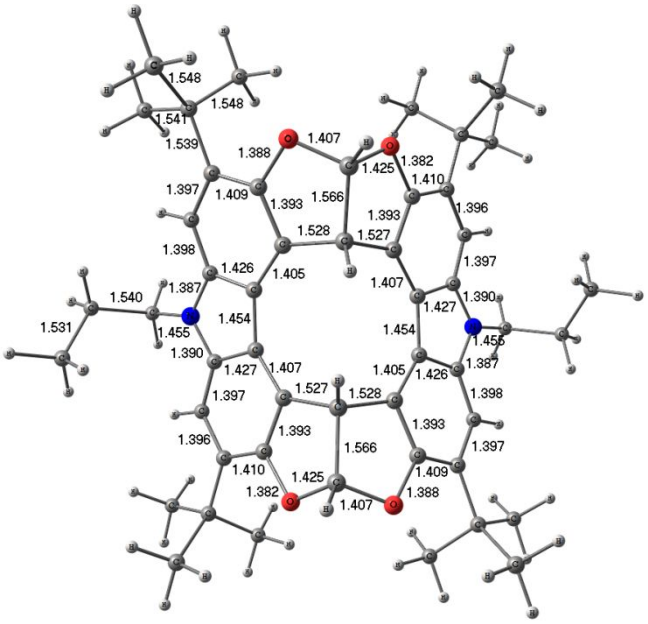

Figure S6: The optimized structure of compound **10** in the ground singlet state calculated at the B3LYP/6-31(d) level of theory.

2.3. Nucleus-Independent Chemical Shifts

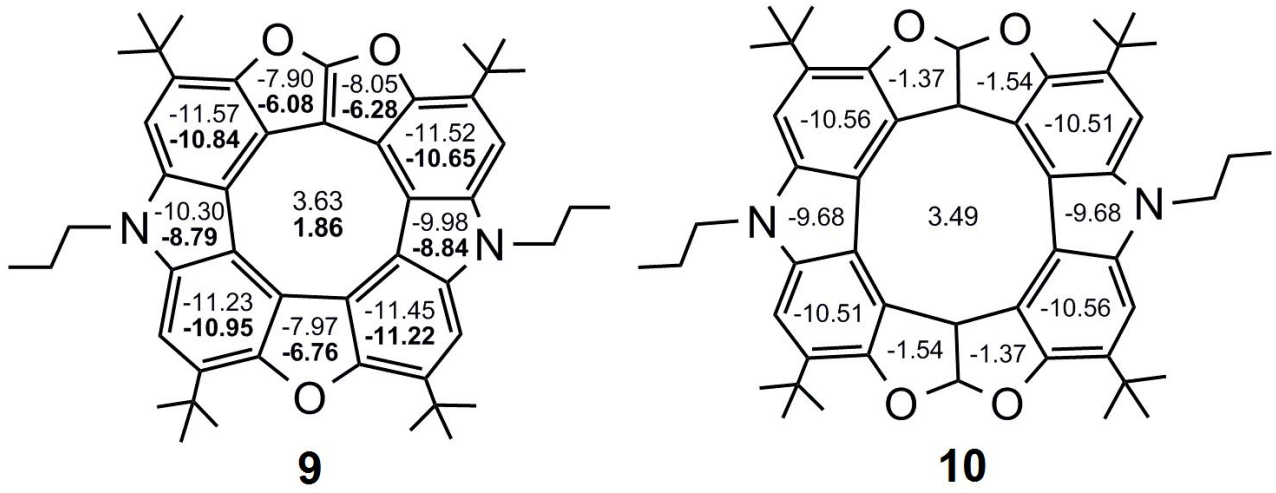

Figure S7: NICS (in ppm) values for the compounds **9** and **10** calculated at the B3LYP/6-311++G(d,p) level of theory.

Significantly lower central ring current of 9 and the corresponding NICS values for the central ring of **9** do not mean the anti-aromatic character of diazadioxa[8]circulene in this context. In our very recent paper (Angew. Chem. Int. ed., 2020, 132, 13, 5182-8188) we have confirmed by 1H NMR analysis an antiaromatic character of nine-membered ring in quite similar dihydro[9]circulene by positioning of aromatic proton directly over the center of nine-membered ring. In that paper we have also introduced the "induced paratropicity" term meaning that paratropic currents inside membered ring are induced by local diatropic currents inside five- and six-membered rings. It means that diazatrioxa[9]circulene is not anti-aromatic as a whole, but induced paratropic currents in the inner 9-membered ring compensate the outer diatropic currents, so the net current should be closed to zero, i.e. diazatrioxa[9]circulene most likely is non-aromatic or weakly aromatic compound. That was shown in many of our previous works for numerous hetero[8]circulenes (Phys. Chem. Chem. Phys., 2014, 16, 15367, Phys. Chem. Chem. Phys., 2016,18, 8980-8992, J. Mol. Model. 2015, 21, 136).

We have measured the average distance from the center of 9-membered rings to radial C atoms equal to 2.12 Å comparing to 1.85 Å in diazadioxa[8]circuelene (see figure below). The difference is quite small (0.27 Å) and of course it affects the smaller NICS values. From another side, the radialene-type structure of diazatrioxa[9]circulene 9 also affect reduced paratropicity in the inner ring in contrast to "annulene-within-annulene" diazadioxa[8]circulene. Both these factors affect smaller NICS values for inner ring of diazatrioxa[9]circulene (NICS(0) and NICS(1) equal to 3.6 and 1.8 ppm, respectively) comparing to diazadioxa[8]circulene (8.26 and 5.08 ppm, J. Mol. Model. 2013, 19, 847). At the same time NICS indices in five and six-membered rings are comparable for both [8]- and [9]circulenes.

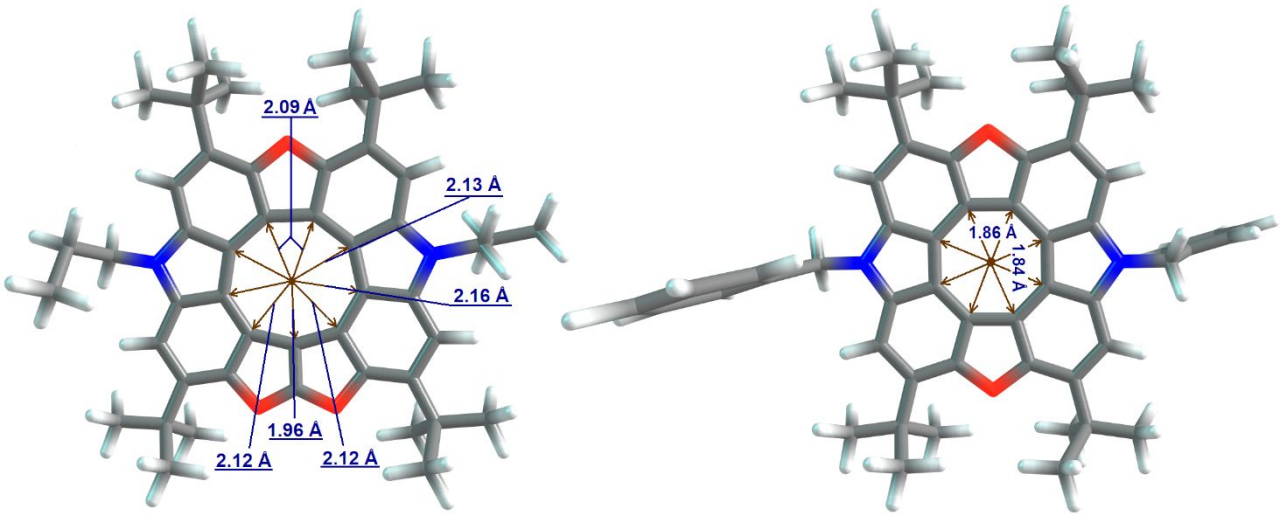

Diazatrioxa[9]circulene

Diazadioxa[8]circulene

We have used the induced current density (ACID) approach which additionally confirms the presence of two concentric ring currents (a diatropic magnetically-induced currents appear in the outer rim, while the 9-membered hub ring sustains paratropic currents) that is typical for the other hetero[8]circulenes (Mol. Phys. 2017, 115, 2218–2230).

2.4. Electronic Absorption Spectra

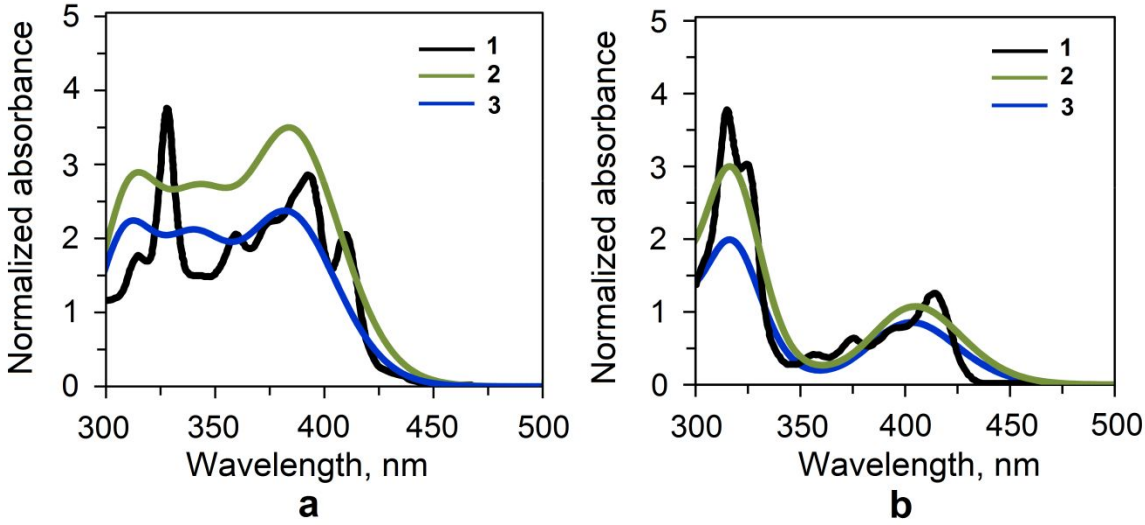

Figure S8: Electronic absorption spectra of the compounds **9** (***a***) and **10** (***b***): **1**– experimental absorption spectrum (recorded in CH_2Cl_2); **2**–calculated by taking into account the solvent effect of CH_2Cl_2, **3**–calculated in vacuum approximation. (Calculations have been performed by the TD DFT/B3LYP/6-31G(d) method; band half-width equals 3000 cm^{-1}, Gaussian distribution function).

Table S1: Wavelengths (λ), oscillator strengths (*f*) and orbital assignment of the selected electronic transitions in the calculated absorption spectra of the circulenes **8**, **9** and **10**.

State	Transition	$\lambda_{vac.}$, $\lambda_{solv.}$, nm	λ_{exp}, nm	$f_{vac.}$, $f_{solv.}$	Assignment
circulene **9**					
S_1	$X^1A \rightarrow 1^1A$	391, 393	410 393	0.1944, 0.2704	HOMO→LUMO (95%)
S_2	$X^1A \rightarrow 2^1A$	376, 378	375	0.1477, 0.2311	HOMO-1→LUMO (91%)
S_3	$X^1A \rightarrow 3^1A$	342, 345	359	0.2388, 0.2932	HOMO→LUMO+1 (88%)
S_4	$X^1A \rightarrow 4^1A$	321, 324		0.0614, 0.1122	HOMO-1→LUMO+1 (90%)
S_5	$X^1A \rightarrow 5^1A$	309, 310		0.1955, 0.2444	HOMO-2→LUMO (90%)
S_6	$X^1A \rightarrow 6^1A$	307, 307		0.0515, 0.0615	HOMO-3→LUMO (94%)
S_7	$X^1A \rightarrow 7^1A$	292, 291		0.0183, 0.0189	HOMO-4→LUMO (91%)
S_8, S_9[a]	$X^1A \rightarrow 8^1A$	277, 276		0.0022, 0.0037	HOMO-5→LUMO (49%) HOMO-2→LUMO+1 (30%)
S_9, S_8[a]	$X^1A \rightarrow 9^1A$	274, 274		0.1108, 0.1606	HOMO-2→LUMO+1 (56%) HOMO-5→LUMO (29%) HOMO→LUMO+3 (9%)
S_{10}	$X^1A \rightarrow 10^1A$	272, 272		0.0109, 0.0128	HOMO→LUMO+2 (70%)

S_{11}	$X^1A \rightarrow 11^1A$	267, 268		0.1393, 0.1809	HOMO-3→LUMO+1 (67%) HOMO→LUMO+2 (18%)
S_{12}	$X^1A \rightarrow 12^1A$	266, 267		0.0121, 0.0246	HOMO-1→LUMO+2 (54%) HOMO→LUMO+3 (20%) HOMO-2→LUMO+1 (19%)
S_{13}	$X^1A \rightarrow 13^1A$	263, 263		0.0498, 0.0394	HOMO-4→LUMO+1 (47%) HOMO-1→LUMO+2 (23%)
S_{14}	$X^1A \rightarrow 14^1A$	250, 252		0.3518, 0.4766	HOMO-4→LUMO+1 (40%) HOMO→LUMO+3 (24%) HOMO-1→LUMO+2 (12%) HOMO→LUMO+5 (11%)
S_{15}	$X^1A \rightarrow 15^1A$	250, 250		0.0084, 0.0014	HOMO→LUMO+4 (44%) HOMO-5→LUMO+1 (28%)
S_{16}, S_{17}[a]	$X^1A \rightarrow 16^1A$	242, 244		0.1895, 0.9864	HOMO→LUMO+5 (69%) HOMO-1→LUMO+6 (12%)
S_{17}, S_{16}[a]	$X^1A \rightarrow 17^1A$	241, 242		0.2821, 0.0124	HOMO-1→LUMO+3 (61%) HOMO-3→LUMO+1 (13%)
S_{18}	$X^1A \rightarrow 18^1A$	240, 241		0.1805, 0.0505	HOMO-5→LUMO+1 (52%) HOMO→LUMO+4 (28%) HOMO-2→LUMO+2 (14%)
S_{19}	$X^1A \rightarrow 19^1A$	234, 235		0.0106, 0.0254	HOMO→LUMO+6 (85%)
S_{20}	$X^1A \rightarrow 20^1A$	233, 234		0.0034, 0.0078	HOMO-1→LUMO+4 (75%)
circulene **10**					
S_1	$X^1A \rightarrow 1^1B$	404, 406	414	0.1168, 0.1464	HOMO→LUMO (99%)
S_2	$X^1A \rightarrow 1^1A$	365, 367		0.0096, 0.0147	HOMO-1→LUMO (98%)
S_3	$X^1A \rightarrow 2^1A$	347, 348		0.0096, 0.0124	HOMO→LUMO+1 (98%)
S_4	$X^1A \rightarrow 3^1A$	330, 329		0.0017, 0.0023	HOMO-2→LUMO (96%)
S_5	$X^1A \rightarrow 2^1B$	324, 326	325	0.0209, 0.0265	HOMO-1→LUMO+1 (98%)
S_6	$X^1A \rightarrow 3^1B$	317, 317	316	0.2422, 0.3740	HOMO-3→LUMO (94%)
S_8	$X^1A \rightarrow 4^1B$	291, 291		0.1330, 0.1668	HOMO-2→LUMO+1 (85%)
S_{10}	$X^1A \rightarrow 7^1A$	280, 281		0.0046, 0.0057	HOMO-3→LUMO+1 (73%) HOMO→LUMO+2 (22%)
S_{11}	$X^1A \rightarrow 5^1B$	269, 271		0.1596, 0.3547	HOMO-1→LUMO+2 (82%)
S_{12}	$X^1A \rightarrow 5^1B$	264, 265		0.1834, 0.2870	HOMO-5→LUMO (58%) HOMO-4→LUMO+1 (14%)
S_{13}	$X^1A \rightarrow 6^1B$	259, 260		0.1574, 0.1955	HOMO→LUMO+3 (66%) HOMO-5→LUMO (27%)
S_{14}	$X^1A \rightarrow 7^1B$	255, 254		0.0091, 0.0123	HOMO-2→LUMO+2 (54%) HOMO→LUMO+4 (39%)
S_{15}	$X^1A \rightarrow 8^1B$	250, 251		0.3903, 0.4245	HOMO-4→LUMO+1 (76%)
S_{16}	$X^1A \rightarrow 8^1A$	249, 250		0.0021, 0.0014	HOMO-1→LUMO+3 (89%)
S_{17}	$X^1A \rightarrow 9^1A$	248, 248		0.0012, 0.0037	HOMO-3→LUMO+2 (71%)
S_{18}	$X^1A \rightarrow 9^1B$	245, 245		0.0842, 0.1061	HOMO→LUMO+4 (54%) HOMO-2→LUMO+2 (38%)
S_{20}	$X^1A \rightarrow 11^1A$	240, 241		0.0037, 0.0042	HOMO→LUMO+5 (60%) HOMO-5→LUMO+1 (27%)
diazadioxa[8]circulene (**8**)					
S_1	$X^1A' \rightarrow {}^1A''$	425, 421	420	0.0003, 0.0007	HOMO-1→LUMO (94%)
S_2	$X^1A' \rightarrow {}^1A'$	397, 403	403	0.2576, 0.3432	HOMO→LUMO (88%)
S_3	$X^1A' \rightarrow {}^1A'$	394, 395	399	0.0017, 0.0002	HOMO-2→LUMO (92%)
S_4	$X^1A' \rightarrow {}^1A''$	371, 374	368	0.3559, 0.4774	HOMO-3→LUMO (87%)
S_5	$X^1A' \rightarrow {}^1A''$	293, 293		0.0001, 0.0001	HOMO-4→LUMO (86%)

S_6	$X^1A' \rightarrow {}^1A'$	279, 279		0.0007, 0.0009	HOMO→LUMO +1 (74%) HOMO-3→LUMO +2 (19%)
S_{10}	$X^1A' \rightarrow {}^1A'$	266, 266		0.2256, 0.2871	HOMO-1→LUMO +2 (61%) HOMO-2→LUMO +1(21%)
S_{11}	$X^1A' \rightarrow {}^1A''$	263, 263	269	0.4012, 0.5181	HOMO-1→LUMO +1 (60%) HOMO-2 →LUMO +2 (20%)
S_{17}, S_{18}[a]	$X^1A' \rightarrow {}^1A''$	233, 235		0.0388, 0.1222	HOMO-7 →LUMO (67%) HOMO→LUMO +3 (22%)
S_{18}, S_{17}[a]	$X^1A' \rightarrow {}^1A''$	231, 232	240	0.7557, 1.0214	HOMO→LUMO +3 (47%) HOMO-7→LUMO (19%)
S_{22}	$X^1A' \rightarrow {}^1A'$	219, 220	226	0.4686, 0.6928	HOMO→LUMO +4 (45%) HOMO-3→LUMO +3 (32%)
S_{23}	$X^1A' \rightarrow {}^1A''$	219, 219		0.1739, 0.1607	HOMO-4→LUMO +1 (40%) HOMO-3→LUMO+4 (32%)

[a]calculations in the frameworks of the PCM model (solvent – CH_2Cl_2).

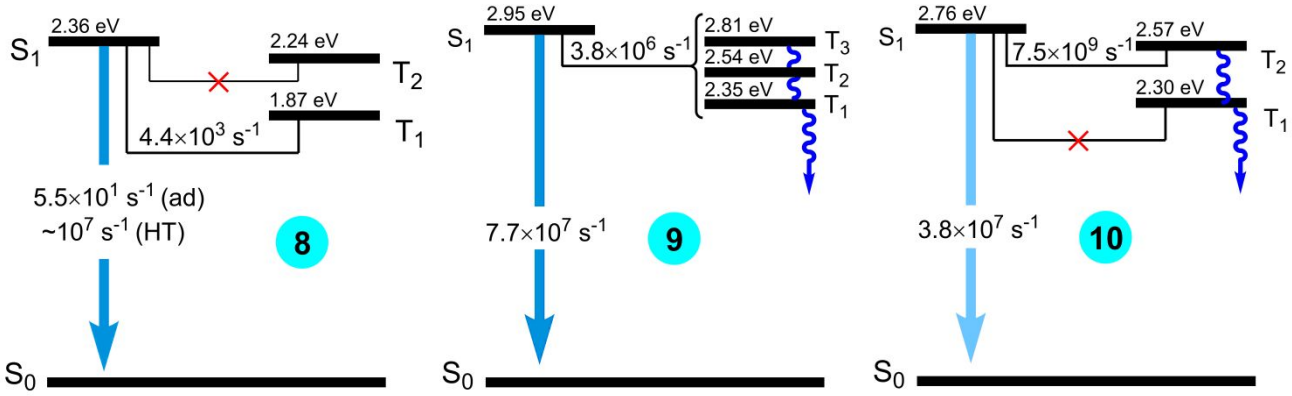

Figure S9: Modified Jablonski diagramfor the circulenes **8**, **9** and **10** calculated by the B3LYP/DZP method in a gas phase approximation based on the S_1 state geometries. The k_r and $k_{S_1 \rightarrow T_j}$ rate constants are also presented here in accordance to Eqs. (7) and (8), respectively, in computational details section.

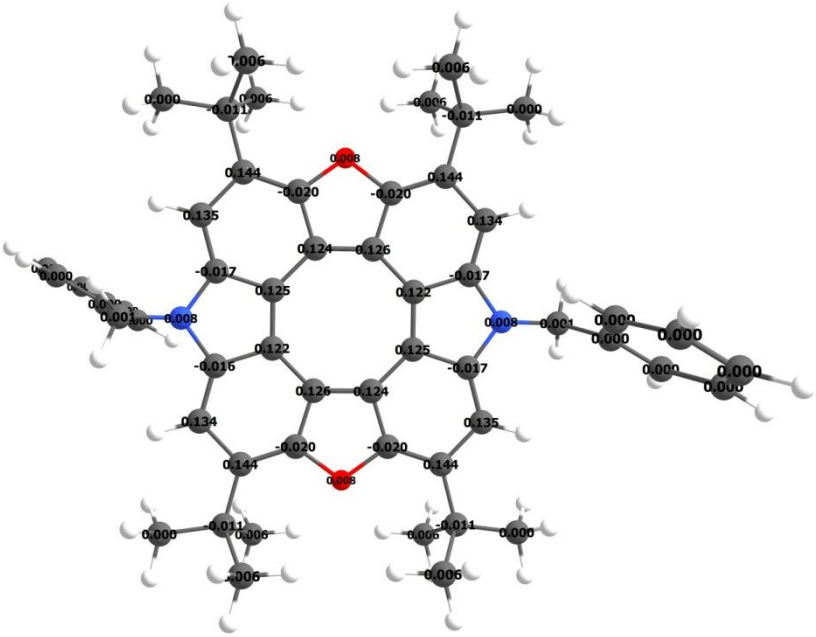

Diazadioxa[9]circulene **(8)**

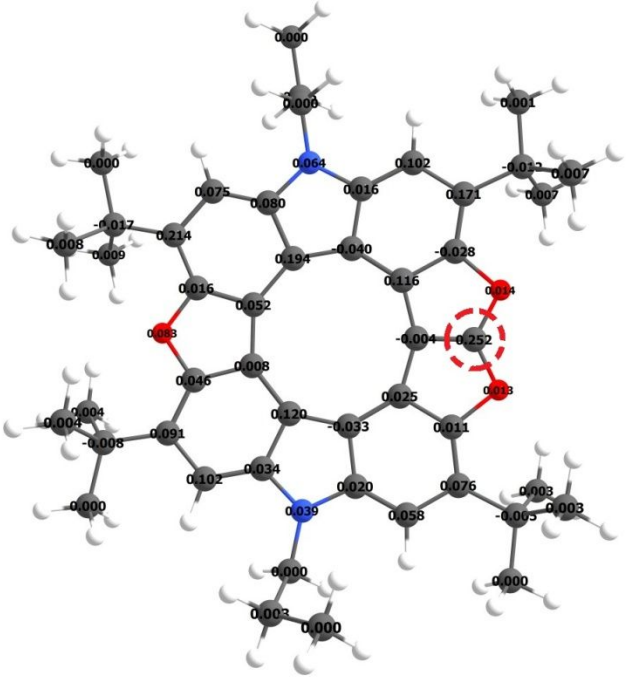

Diazatrioxa[9]circulene **(9)**

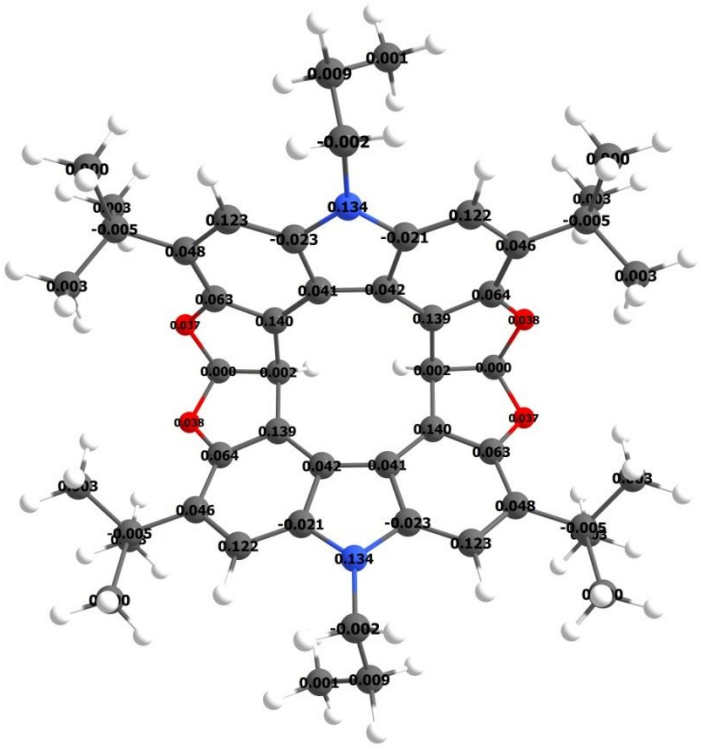

Tetrahydro-diazatetraoxa[10]circulene (**10)**

Figure S10: Mulliken atomic spin densities with summated Hydrogen contributions calculated by the UB3LYP/6-31G(d) method in T_1 state of circulenes **8**, **9** and **10**.

Further comments on optical properties

It has previously been established [39,40] that for the symmetrical hetero[8]circulenes, e.g. (7) or (8), the fluorescence is forbidden in the electric-dipole approximation, but accounting for Herzberg-Teller vibronic coupling the S_1-S_0 transition gains an intensity (f=0.01) high enough to demonstrate a clear blue fluorescence. At the same time, the ISC channel of the S_1 state deactivation for [8]circulenes (7) or (8) is very slow and S_1~S_0 radiationless internal conversion is a main competing process to the fluorescence one. For [9]circulene (**9**) the S_1-S_0 transition is well allowed in the electric-dipole approximation (f=0.21) which corresponds to the prompt blue fluorescence even in the adiabatic approximation without accounting of vibronic effects. The calculated ISC rate for [9]circulene (9) is twenty times slower relative to the fluorescence rate, thus this compound demonstrates bright blue fluorescence quenched mainly by the S_1~S_0 internal conversion similarly to circulene (8). In contrast, ISC is very efficient in the case of tetrahydro[10]circulene (10). That is why, despite the quite high intensity of the S_1-S_0 transition (f=0.12) circulene (10) demonstrates a weak fluorescence.

In the case of [9]circulene the effective conjugation length is smaller than [8]circulene that can be seen from corresponding molecular orbitals involved into the electronic transitions (see ESI, Fig. S11). This is because of significant contribution from a [9]radialene structure that is discussed in

details in the main manuscript. Additionally, we have calculated the bond length alternation parameter (ΔR) for the central 9- and 8-membered ring in [9]circulene and [8]circulene molecules. It was found that for [9]circulene ΔR is 0.027 Å which is somewhat larger than that calculated for [8]circulene (ΔR = 0.021 Å). This indicates higher localization of MOs in the [9]circulene (see ESI, Fig. S11) and smaller conjugation length than in [8]circulene (Chem. Eur. J. 2013, 19, 17097).

It should be noted that for the [9]circulene and [8]circulene the absorption bands in spectra have different absorption nature. In the case of [9]circulene the first $S_0 \rightarrow S_1$ electronic transition is strongly allowed ($f_{vac.}$ =0.1944, $f_{solv.}$ =0.2704, Table S1, ESI) due to the main contribution of the HOMO→LUMO configuration. In the electronic spectra of [8]circulene the first $S_0 \rightarrow S_1$ transition has a very low intensity ($f_{vac.}$ =0.0003, $f_{solv.}$ =0.0007, Table S1, ESI) but in the experimental spectra the band of medium intensity at 420 nm is observed. In our previous paper (Chem. Phys., 2015, 459, 65–71) was shown that this is due to the clear manifestation of vibronic effects, which lead to a strong mixing between the first and second excited closely lying states of ^{1}A" and ^{1}A' symmetry, respectively. Vibronic mixing is determined by one-electron vibronic coupling between quasi-degenerate HOMO and HOMO-1 and leads to effective borrowing of intensity by the first $X^1A' \rightarrow {}^1A''$ transition from the more intense second $X^1A' \rightarrow {}^1A'$ transition ($f_{vac.}$ =0.2576, $f_{solv.}$ =0.3432, Table S1, ESI).

2.5. Molecular Orbital Diagrams

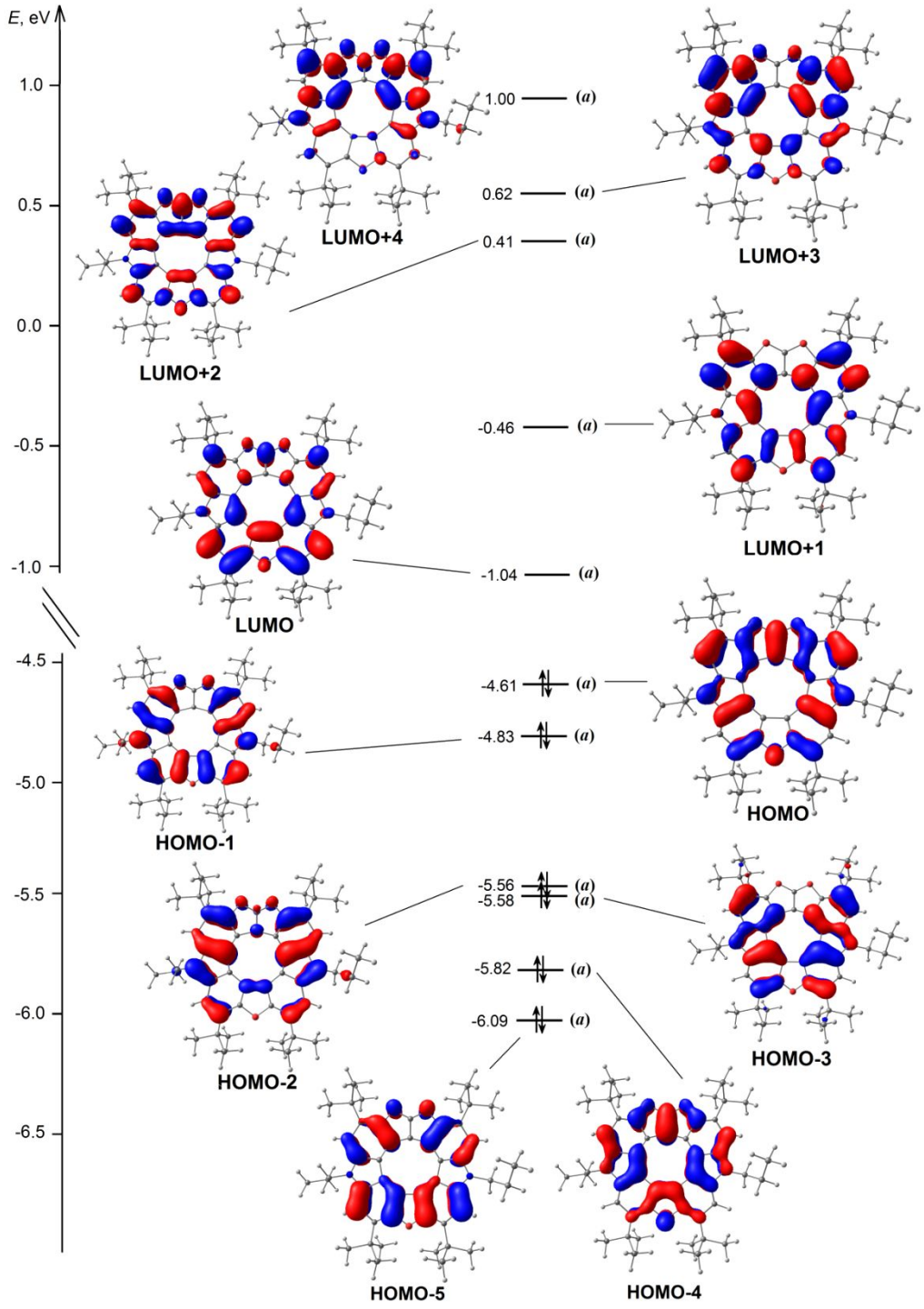

Figure S11: Molecular orbital diagram of the compound **9** calculated at the B3LYP/6-31G(d) level of theory (controlling value of the isosurface is 0.03 a.u.).

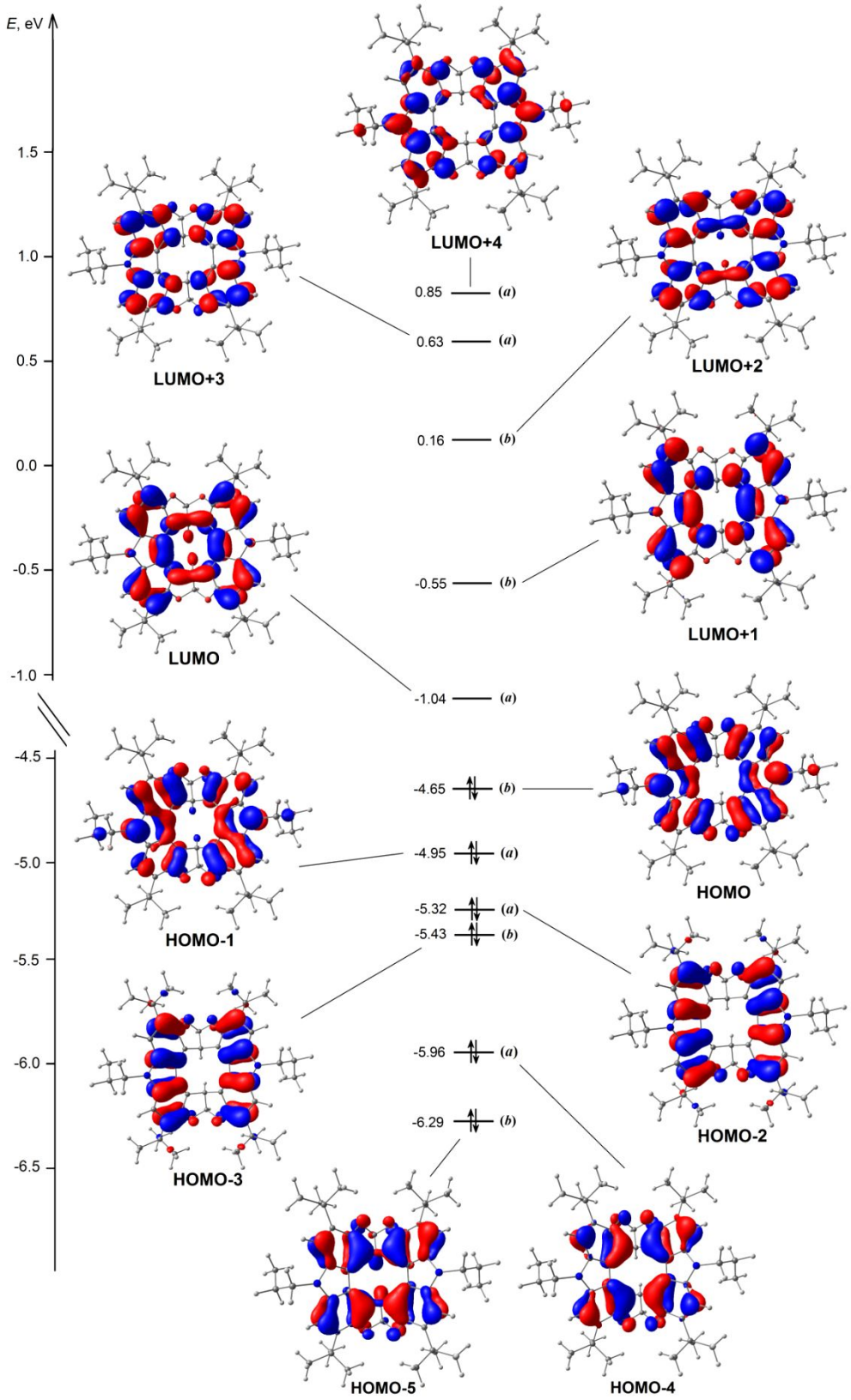

Figure S12: Molecular orbital diagram of the compound **10** calculated at the B3LYP/6-31G(d) level of theory (controlling value of the isosurface is 0.03 a.u.).

2.6. Charge-Transport Properties

In order to further studyof the properties of the circulenes **9** and **10**, we investigated its electron/hole hopping properties computationally. Five different types of intermolecular pair couplings exist in the solid state for each circulene as follows from SCXRD data (dimers **A-E**, Figures S13 and S14). The dimeric pairs **A-E** were chosen in such a way as to cover the main possible carrier transport pathways in the crystal structures of **9** and **10**.

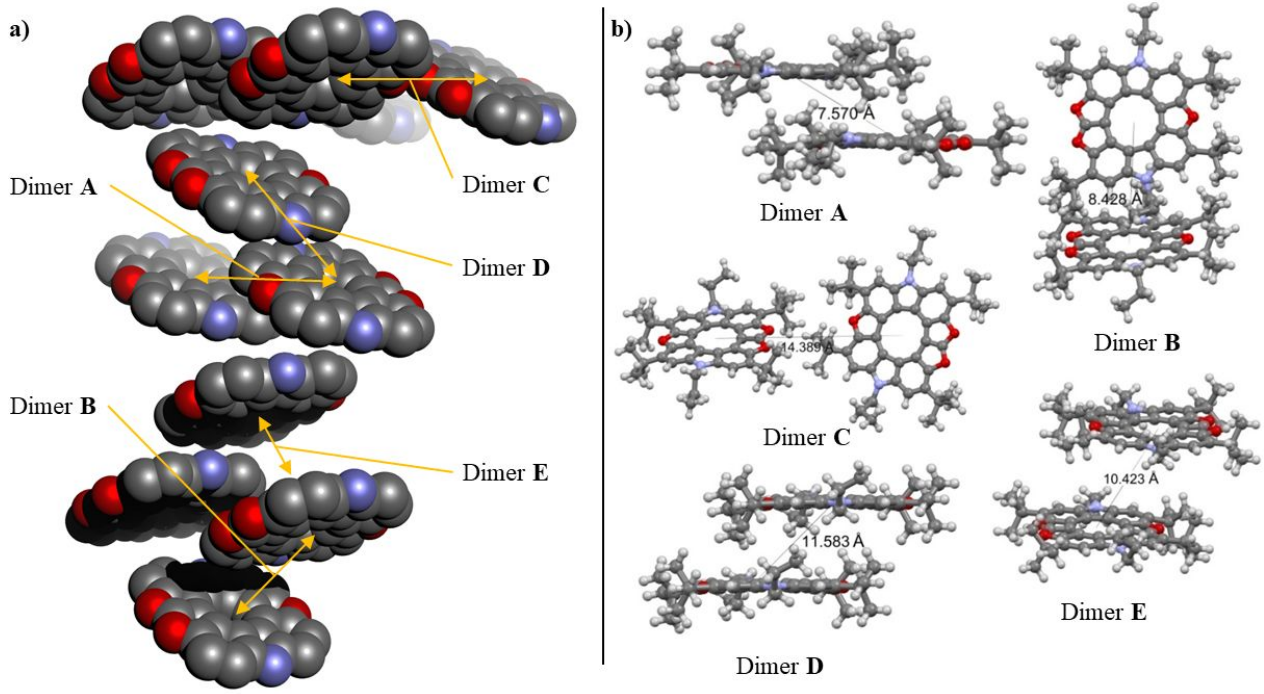

Figure S13: Pertinent dimers extracted from the crystal structure of **9**. a) Dimers shown in the crystal packing of **9**, and b) individual dimers with marked intermolecular centre-to-centre distances

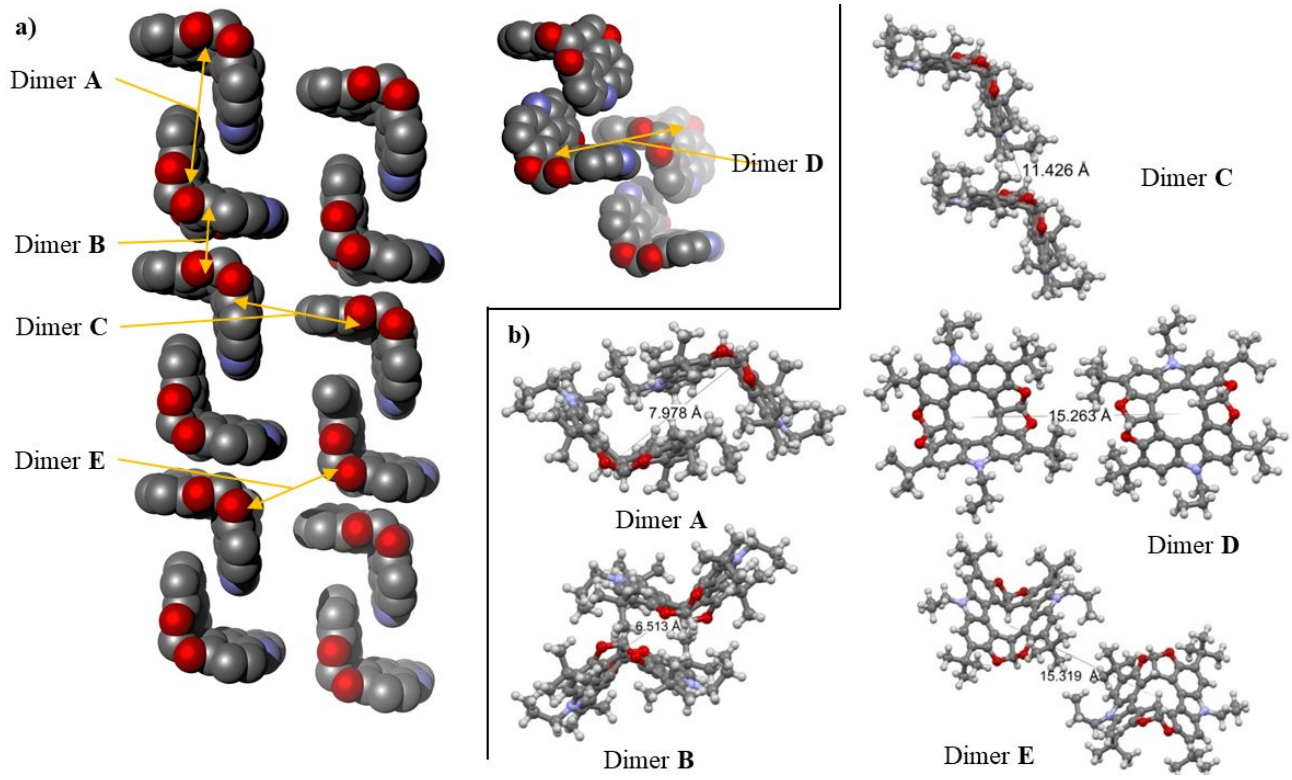

Figure S14: Pertinent dimers extracted from the crystal structure of **10**. a) Dimers shown in the crystal packing of **10**, and b) individual dimers with marked intermolecular centre-to-centre distances.

An obvious characteristic in the molecular structure of **9** is the high planarity of its macrocyclic core. According to the Marcus–Hush theory the charge transfer mobility is dependent on three factors including the reorganization energy λ_+/λ_-, the electronic coupling V and the intermolecular center-of-mass distance d. Thus, among five separated dimers (**A–E**) of compound **9** the integral transfer (V) only for the first dimer **A** with π-π stacking interactions and the shortest intermolecular center-of-mass distance d (7.57 Å) has significantly larger values (V_h = 7.58 meV and V_e = 8.35 meV) compared to that for the other dimers (**B–E**). This is due to more complicated charge transfer in dimers **B–E** in which molecules are more distant and oriented at certain angles to one another which prevents effective spatial overlap of the molecular orbitals of the neighboring molecules in dimers. Using the Marcus-Hush charge transport theory, the hole and electron mobility values in **9** were calculated to be 0.013 and 0.038 $cm^2\ V^{-1}\ s^{-1}$, respectively (Table S2).

Table S2: The intermolecular center-of-mass distance d (in Å), hole and electron reorganization energies λ_h/λ_e (eV), integral transfer V (meV), rate of charge hopping k (s^{-1}) and charge transfer mobility μ_h and μ_e (in $cm^2\ V^{-1}\ s^{-1}$) of circulenes **9** and **10** calculated at the B3LYP/DZP theory level

Compound	Dimer	d	Reorganization energy		Integral transfer		Rate of charge hopping		Charge transfer mobility	
			Hole	Electron	Hole	Electron	Hole	Electron	Hole (μ_h)	Electron (μ_e)
9	**A**	7.570	0.178	0.118	7.58	8.35	4.05×10^{11}	1.08×10^{12}	0.013	0.038
	B	8.428			2.46	1.48	4.27×10^{10}	3.39×10^{10}		
	C	14.389			0.48	−1.36	1.62×10^{9}	2.86×10^{10}		
	D	11.583			1.66	0.06	1.94×10^{10}	5.57×10^{7}		
	E	10.423			−0.05	0.21	1.76×10^{7}	6.82×10^{8}		
10	**A**	7.978	0.171	0.203	25.66	7.39	5.08×10^{12}	2.82×10^{11}	0.163	0.009
	B	6.513			−18.52	7.41	2.64×10^{12}	2.84×10^{11}		
	C	11.426			0.22	3.33	3.73×10^{8}	5.74×10^{10}		
	D	15.263			0.03	1.47	6.94×10^{6}	1.12×10^{10}		
	E	15.319			0.06	0.94	2.78×10^{7}	4.57×10^{9}		

In the case of compound **10,** the hole mobility is predicted at the level of 0.163 $cm^2\ V^{-1}\ s^{-1}$ that is significantly larger than that for the electron mobility 0.009 $cm^2\ V^{-1}\ s^{-1}$(Table S2). In the viewpoint of transfer integral (V), the electron coupling among the dominant hopping pathways indicates that the charge transport processes mainly take place in the parallel dimers (**A** and **B**) with π-π interactions.

2.7. Optimized Cartesian Coordinates

Table S3: The optimized Cartesian coordinates for the compound **9** in the ground singlet state calculated at the B3LYP/6-31(d) level of theory

Center Number	Atomic Number	Coordinates (Angstroms) X	Y	Z
1	8	-2.815674	-3.397213	-0.169949
2	8	1.498436	3.505849	-0.031223
3	8	-0.645653	-4.347729	0.037365
4	7	3.885055	-1.334712	0.356957
5	7	-3.688704	1.985614	-0.300857
6	6	7.459460	-2.261507	-0.744858
7	1	8.018375	-1.481600	-0.213001
8	1	7.934685	-2.402424	-1.721307
9	1	7.576091	-3.195201	-0.180801
10	6	5.983242	-1.884479	-0.899592
11	1	5.886926	-0.961531	-1.484787
12	1	5.450332	-2.663201	-1.459119
13	6	5.290758	-1.688075	0.458141
14	1	5.365494	-2.602985	1.055848
15	1	5.799933	-0.908713	1.035505
16	6	3.377759	-0.051365	0.240103
17	6	1.951055	-0.076765	0.132878
18	6	1.302022	1.209249	0.035774
19	6	-0.059778	1.805729	-0.063682
20	6	-1.447010	1.411574	-0.138702
21	6	-2.396840	2.478421	-0.215795
22	6	-4.886155	2.804318	-0.424460
23	1	-5.661128	2.193587	-0.897217
24	1	-4.668217	3.617552	-1.126542
25	6	-5.404796	3.385695	0.902690
26	1	-4.608387	3.981389	1.365229
27	1	-6.216512	4.085416	0.660237
28	6	-5.904794	2.335602	1.898769
29	1	-6.752789	1.771361	1.491486
30	1	-6.238316	2.810121	2.828215
31	1	-5.116791	1.619064	2.151810
32	6	2.837254	-2.224911	0.290014
33	6	2.942691	-3.622442	0.334081
34	1	3.920939	-4.076159	0.419694
35	6	1.806429	-4.428530	0.256055
36	6	0.610981	-3.712170	0.134780
37	6	0.465277	-2.297632	0.086604
38	6	-0.945444	-2.074215	-0.045005
39	6	-1.490432	-3.323237	-0.063325
40	6	-3.203690	-2.041182	-0.225383
41	6	-4.542068	-1.648195	-0.327661
42	6	-4.725071	-0.265582	-0.351800
43	1	-5.724548	0.141677	-0.413476
44	6	-3.630460	0.608654	-0.282021
45	6	-2.264702	0.206024	-0.181162
46	6	-2.068428	-1.187507	-0.149756
47	6	2.183070	2.326952	0.040075
48	6	0.166742	3.211035	-0.086329
49	6	-0.776405	4.259146	-0.142695
50	6	-0.410044	5.754631	-0.084737
51	6	-1.655771	6.651972	-0.242285
52	1	-1.347493	7.702756	-0.208125
53	1	-2.382111	6.499631	0.564029
54	1	-2.162093	6.487284	-1.200465
55	6	0.564478	6.132791	-1.223940
56	1	1.511821	5.600927	-1.143891
57	1	0.775742	7.208766	-1.193487
58	1	0.125120	5.903297	-2.201803
59	6	0.218092	6.076846	1.292287
60	1	1.098124	5.463128	1.492057
61	1	-0.504872	5.897037	2.096457
62	1	0.518484	7.131129	1.336166
63	6	-2.093077	3.839940	-0.211946

64	1	-2.896595	4.560851	-0.258092
65	6	3.593023	2.342837	0.098972
66	6	4.174897	1.092688	0.210850
67	1	5.249761	0.989950	0.259983
68	6	1.618405	-1.494912	0.160873
69	6	4.445174	3.622423	-0.001116
70	6	5.950921	3.317194	0.144377
71	1	6.186478	2.864345	1.114401
72	1	6.514769	4.253777	0.071879
73	1	6.317931	2.653857	-0.646936
74	6	4.239650	4.268055	-1.392584
75	1	4.588007	3.594184	-2.183948
76	1	4.811124	5.201620	-1.466469
77	1	3.189654	4.494413	-1.585605
78	6	4.077243	4.623922	1.117701
79	1	3.043094	4.957781	1.041297
80	1	4.724588	5.507427	1.056672
81	1	4.218069	4.170243	2.105791
82	6	-5.705829	-2.651489	-0.394777
83	6	-5.545318	-3.559831	-1.638169
84	1	-5.546121	-2.963509	-2.557938
85	1	-6.380436	-4.268898	-1.693882
86	1	-4.616010	-4.133148	-1.604918
87	6	-7.067391	-1.938150	-0.503413
88	1	-7.266240	-1.300015	0.365298
89	1	-7.866211	-2.686530	-0.551691
90	1	-7.136467	-1.322724	-1.407707
91	6	-5.725075	-3.518609	0.887705
92	1	-4.801474	-4.090027	1.005227
93	1	-6.561060	-4.227843	0.848181
94	1	-5.854995	-2.892060	1.777765
95	6	1.861344	-5.965037	0.292983
96	6	1.051985	-6.490536	1.503787
97	1	1.101745	-7.585807	1.540850
98	1	-0.000004	-6.201714	1.445201
99	1	1.461340	-6.101639	2.443360
100	6	3.307349	-6.478998	0.431719
101	1	3.933901	-6.170897	-0.413150
102	1	3.302992	-7.574345	0.456721
103	1	3.778559	-6.129477	1.357462
104	6	1.274801	-6.543417	-1.017968
105	1	1.846768	-6.196067	-1.886234
106	1	0.231413	-6.252007	-1.158810
107	1	1.322127	-7.639160	-0.997991

Table S4: The optimized Cartesian coordinates for the compound **10** in the ground singlet state calculated at the B3LYP/6-31(d) level of theory

Center Number	Atomic Number	Coordinates (Angstroms) X	Y	Z
1	8	-3.403900	2.294083	1.226992
2	8	-4.045071	0.158752	1.777478
3	8	4.045071	-0.158752	1.777478
4	8	3.403900	-2.294083	1.226992
5	7	1.323383	3.535931	-1.165944
6	7	-1.323383	-3.535931	-1.165944
7	6	1.275923	6.580180	-0.328973
8	1	0.458886	6.985661	-0.938412
9	1	1.733753	7.417364	0.209588
10	1	0.837177	5.904550	0.412050
11	6	2.314624	5.861789	-1.194212
12	1	3.149087	5.529924	-0.564639
13	1	2.738519	6.563661	-1.925754
14	6	1.772049	4.654513	-1.981713
15	1	0.934337	4.962265	-2.615753
16	1	2.549117	4.280734	-2.659712
17	6	0.018445	3.260311	-0.775459
18	6	-0.000587	2.088158	0.037974
19	6	-1.232848	1.762703	0.633921

20	6	-1.687452	0.629193	1.549918
21	1	-1.006373	0.461910	2.390960
22	6	-2.099425	-0.659020	0.839576
23	6	-1.382194	-1.654904	0.155133
24	6	-2.161186	-2.612900	-0.558185
25	6	-1.772049	-4.654513	-1.981713
26	1	-0.934337	-4.962265	-2.615753
27	1	-2.549117	-4.280734	-2.659712
28	6	-2.314624	-5.861789	-1.194212
29	1	-3.149087	-5.529924	-0.564639
30	1	-2.738519	-6.563661	-1.925754
31	6	-1.275923	-6.580180	-0.328973
32	1	-0.458886	-6.985661	-0.938412
33	1	-1.733753	-7.417364	0.209588
34	1	-0.837177	-5.904550	0.412050
35	6	-2.314624	2.618858	0.441705
36	6	-2.331380	3.742939	-0.409654
37	6	-3.590304	4.605735	-0.607016
38	6	-3.353549	5.741620	-1.621636
39	1	-2.578294	6.440203	-1.285401
40	1	-4.278728	6.315438	-1.745606
41	1	-3.068548	5.357907	-2.608256
42	6	-4.747562	3.728017	-1.141913
43	1	-4.484817	3.288943	-2.111525
44	1	-5.648466	4.338710	-1.280251
45	1	-4.987781	2.916091	-0.452179
46	6	-4.001737	5.251531	0.738833
47	1	-4.221401	4.495660	1.495489
48	1	-4.897852	5.869230	0.600007
49	1	-3.201862	5.898014	1.119135
50	6	-1.117058	4.031852	-1.034412
51	1	-1.035884	4.897531	-1.678110
52	6	-3.084213	1.156193	2.023433
53	1	-3.162773	1.441887	3.074489
54	6	-3.559181	-2.626149	-0.555126
55	1	-4.085554	-3.381074	-1.124425
56	6	-4.275098	-1.710913	0.219851
57	6	-5.810293	-1.728708	0.322277
58	6	-6.231697	-1.987196	1.789724
59	1	-5.857926	-2.957942	2.136616
60	1	-7.325948	-1.998767	1.869304
61	1	-5.849083	-1.213818	2.459202
62	6	-6.385638	-0.372920	-0.154964
63	1	-6.008448	0.456672	0.446722
64	1	-7.480133	-0.382760	-0.079930
65	1	-6.120893	-0.186444	-1.202371
66	6	-6.429530	-2.838017	-0.549887
67	1	-6.191385	-2.706440	-1.611826
68	1	-7.520435	-2.810234	-0.451446
69	1	-6.097225	-3.836561	-0.242619
70	6	-3.486836	-0.768802	0.909219
71	6	-0.018445	-3.260311	-0.775459
72	6	1.117058	-4.031852	-1.034412
73	1	1.035884	-4.897531	-1.678110
74	6	2.331380	-3.742939	-0.409654
75	6	3.590304	-4.605735	-0.607016
76	6	4.747562	-3.728017	-1.141913
77	1	4.484817	-3.288943	-2.111525
78	1	5.648466	-4.338710	-1.280251
79	1	4.987781	-2.916091	-0.452179
80	6	3.353549	-5.741620	-1.621636
81	1	2.578294	-6.440203	-1.285401
82	1	4.278728	-6.315438	-1.745606
83	1	3.068548	-5.357907	-2.608256
84	6	4.001737	-5.251531	0.738833
85	1	4.221401	-4.495660	1.495489
86	1	4.897852	-5.869230	0.600007
87	1	3.201862	-5.898014	1.119135
88	6	2.314624	-2.618858	0.441705
89	6	1.232848	-1.762703	0.633921
90	6	1.687452	-0.629193	1.549918
91	1	1.006373	-0.461910	2.390960
92	6	3.084213	-1.156193	2.023433
93	1	3.162773	-1.441887	3.074489

94	6	3.486836	0.768802	0.909219
95	6	2.099425	0.659020	0.839576
96	6	1.382194	1.654904	0.155133
97	6	2.161186	2.612900	-0.558185
98	6	3.559181	2.626149	-0.555126
99	1	4.085554	3.381074	-1.124425
100	6	4.275098	1.710913	0.219851
101	6	5.810293	1.728708	0.322277
102	6	6.231697	1.987196	1.789724
103	1	5.857926	2.957942	2.136616
104	1	7.325948	1.998767	1.869304
105	1	5.849083	1.213818	2.459202
106	6	6.429530	2.838017	-0.549887
107	1	6.191385	2.706440	-1.611826
108	1	7.520435	2.810234	-0.451446
109	1	6.097225	3.836561	-0.242619
110	6	6.385638	0.372920	-0.154964
111	1	6.008448	-0.456672	0.446722
112	1	7.480133	0.382760	-0.079930
113	1	6.120893	0.186444	-1.202371
114	6	0.000587	-2.088158	0.037974

3. X-ray crystallography

X-ray crystallography was performed by the crystallography service of the Department of Chemistry, University of Copenhagen, Denmark on a Bruker/Nonius Kappa CCD 4-circle diffractometer.

The crystals of **9** used for single x-ray diffraction were produced by slow evaporation from ether and acetonitrile and the crystals of **10** by slow evaporation from ether and ethanol. The single-crystal x-ray diffraction data was collected at 122 K. The instrument is a Bruker D8 Venture equipped with an IμS microfocus source, a KAPPA goniometer, an Oxford Cryosystems nitrogen cryostream cooling device and a PHOTON 100 CMOS, using CuKα radiation.

The diffraction data was reduced using Apex3[5] and later solved using the freeware available software Olex2.[6] The data was solved using the olex2.solve structure solution program[6] together with the method Charge Flipping. Afterward, the refinement was performed using the XL refinement package using the refined using the SHELXL2013 software package.[7]

The hydrogen atoms where attached to the structure as riding atoms. All the non-hydrogen atoms were refined anisotropically.

Crystal data, data collection, and structure refinement statistics are given below for compound **9** and **10**.

Diazatrioxa[9]circulene (**9**)

A structural check has been run on the CIF file and no A or B alert were found.

All the crystal data and refinement for **9** is found in the table below. A structural figure with probability ellipsoids is also shown below.

The CCDC number is: 2005492.

Crystal data and structure refinement for 9	
Identification code	D8V3984_0m1a_a
Empirical formula	$C_{48}H_{54}N_2O_3$
Formula weight	706.93
Temperature/K	122
Crystal system	orthorhombic
Space group	Pbca
a/Å	23.5452(7)
b/Å	11.5828(3)
c/Å	28.4356(10)
α/°	90
β/°	90
γ/°	90
Volume/Å^3	7754.9(4)
Z	8
ρ_{calc}g/cm^3	1.211
μ/mm^{-1}	0.075
F(000)	3040.0
Radiation	MoKα (λ = 0.71073)
2Θ range for data collection/°	4.492 to 50.052
Index ranges	-28 ≤ h ≤ 27, -13 ≤ k ≤ 13, -33 ≤ l ≤ 33
Reflections collected	55914
Independent reflections	6838 [R_{int} = 0.0906, R_{sigma} = 0.0410]
Data/restraints/parameters	6838/0/492
Goodness-of-fit on F^2	1.029
Final R indexes [I>=2σ (I)]	R_1 = 0.0435, wR_2 = 0.0954
Final R indexes [all data]	R_1 = 0.0718, wR_2 = 0.1093
Largest diff. peak/hole / e Å^{-3}	0.22/-0.28

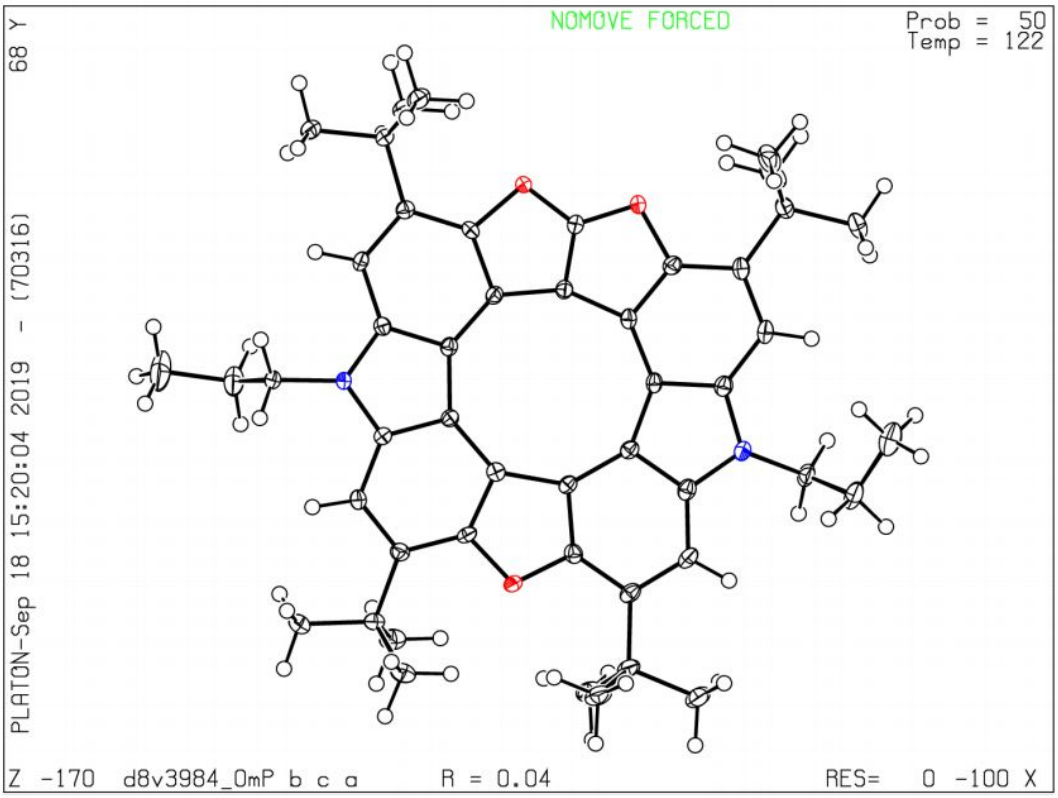
NOMOVE FORCED
Prob = 50
Temp = 122
68 Y
PLATON-Sep 18 15:20:04 2019 - (70316)
Z -170 d8v3984_0mP b c a
R = 0.04
RES= 0 -100 X

Tetrahydro-diazatetraoxa[9]circulene (**10**)

A structural check has been run on the CIF file and no A or B alert were found.

All the crystal data and refinement for **10** is found in the table below. A structural figure with probability ellipsoids is also shown below.

The CCDC number is: 2005493.

Crystal data and structure refinement for **10**	
Identification code	D8V4065_0m1_a
Empirical formula	$C_{50}H_{58}N_2O_4$
Formula weight	750.98
Temperature/K	122
Crystal system	triclinic
Space group	P-1
a/Å	11.4260(14)
b/Å	14.3687(17)
c/Å	15.1478(18)
α/°	103.508(4)
β/°	108.336(4)
γ/°	109.432(4)
Volume/Å^3	2061.1(4)
Z	2
ρ_{calc}g/cm^3	1.210
μ/mm^{-1}	0.076
F(000)	808.0
Radiation	MoKα (λ = 0.71073)
2Θ range for data collection/°	4.69 to 59.15
Index ranges	-15 ≤ h ≤ 15, -19 ≤ k ≤ 19, -21 ≤ l ≤ 21
Reflections collected	45231
Independent reflections	11517 [R_{int} = 0.0427, R_{sigma} = 0.0414]
Data/restraints/parameters	11517/0/519
Goodness-of-fit on F^2	1.012
Final R indexes [I>=2σ (I)]	R_1 = 0.0469, wR_2 = 0.1124
Final R indexes [all data]	R_1 = 0.0680, wR_2 = 0.1234
Largest diff. peak/hole / e Å^{-3}	0.37/-0.28

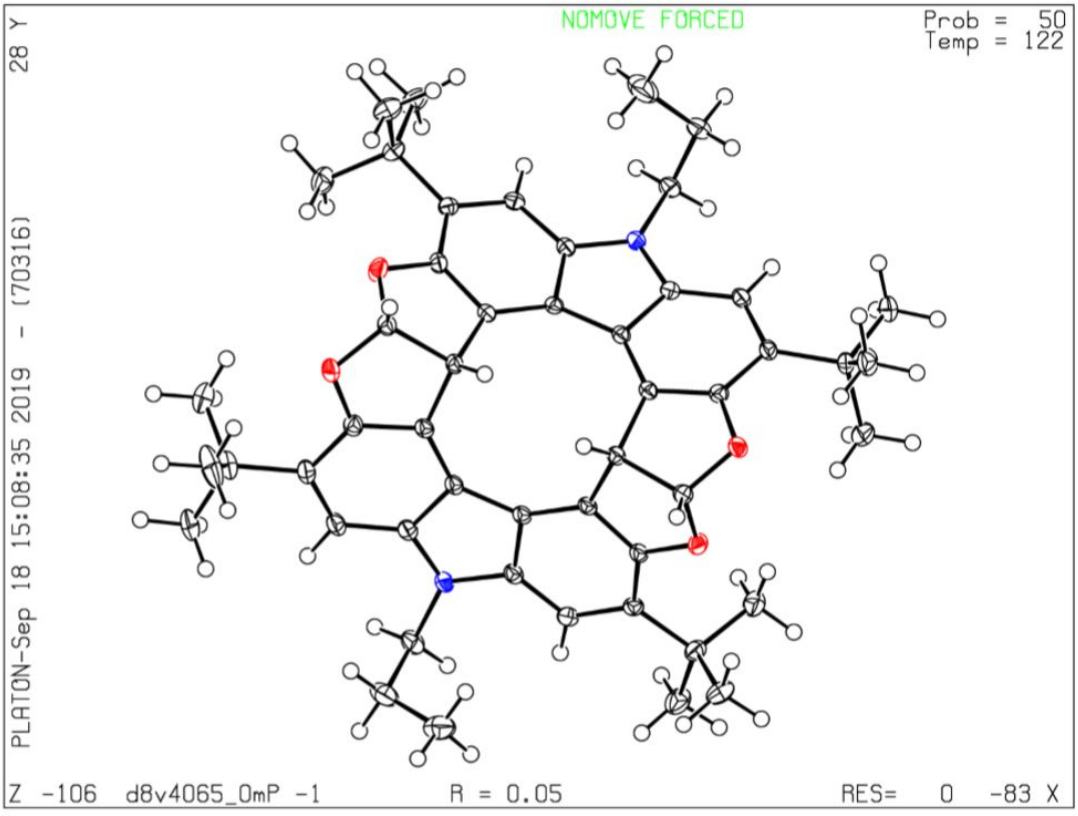
NOMOVE FORCED
Prob = 50
Temp = 122
28 Y
PLATON-Sep 18 15:08:35 2019 - (70316)
Z -106 d8v4065_0mP -1
R = 0.05
RES= 0 -83 X

4. General Experimental Procedures

General Methods. All chemicals, unless otherwise stated, were purchased from commercial suppliers and used as received. All solvents were high-performance liquid chromatography (HPLC) grade. Analytical thin-layer chromatography (TLC) was performed on SiO_2 60 F254 0.2 mm-thick precoated TLC plates. Flash column vacuum chromatography was performed using SiO_2 (SI 1721, 60 Å, 40-63 µm, respectively). Melting points (mp) are uncorrected. ^1H NMR and ^{13}C NMR spectra were recorded at 500 and 125 MHz, respectively, using residual nondeuterated solvent as the internal standard. All chemical shifts (δ) are quoted in ppm, and all coupling constants (J) are expressed in hertz (Hz). The following abbreviations are used for convenience in reporting the multiplicity for NMR resonances: s = singlet, bs = broad singlet, d = doublet, t = triplet, q = quartet, sxt = sextet and m = multiplet. High-resolution mass spectrometry (HRMS) spectra were recorded on an ESP-MALDI-FT-ICR instrument equipped with a 7T magnet (prior to the experiments, the instrument was calibrated using NaTFA cluster ions). UV−vis absorption and fluorescence measurements were performed in a 1 cm path-length quartz cuvette, and the neat solvent was used as baseline. Fluorescence quantum yields were determined using 9,10-diphenylanthracene as a standard. Cyclic voltammetry (CV) and differential pulse voltammetry (DPV) were carried out in CH_2Cl_2 containing Bu_4NPF_6 (0.1 M) as the supporting electrolyte using an Autolab PGSTAT12 instrument controlled by the Nova 1.11 software. The working electrode was circular glassy carbon disk (d = 3 mm), the counter electrode was a platinum wire and the reference electrode was a silver wire immersed in the solvent-supporting electrolyte mixture and physically separated from the solution containing the substrate by a ceramic frit. The potential of the reference electrode was determined *vs* the ferrocene/ferrocenium (Fc/Fc^+) redox couple in separate experiments. The voltage sweep rate was 0.1 Vs^{-1} and *iR*-compensation was used in all experiments. Solutions were purged with argon saturated with solvent for at least ten minutes before the measurements were made. During the measurements a stream of argon was maintained over the solutions. The temperature was ~297 K. The substrate concentration was 1.61 mM.

5. Experimental Section

Synthesis of **12**

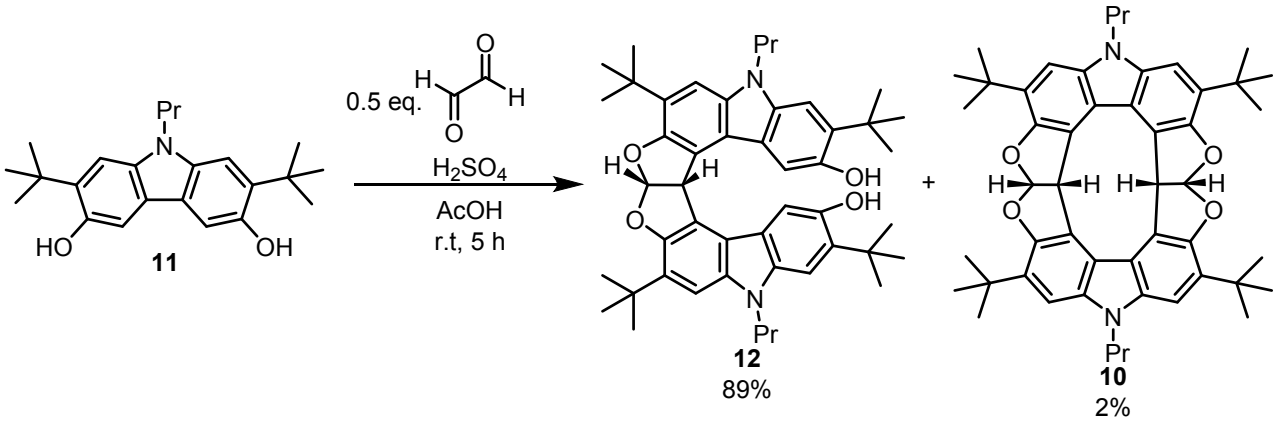

Procedure: To a round bottomed flask, equipped with a magnetic stir bar, was added **11** (2.00 g, 5.66 mmol, 1.0 eq.) and glacial AcOH (113 mL), the suspension was sonicated until complete dissolution. To the stirred solution was added aq. glyoxal (40wt% in H_2O, 0.325 ml, 2.83 mmol, 0.50 eq.) along with concentrated H_2SO_4 (1.13 ml, 21.2 mmol, 3.75 eq.), and the reaction was stirred for 5 hours. To the completed reaction, was added water (150 mL) and EtOAc(150 mL), the aqueous layer separated, and the organic fraction was washed three times with water (3x150 mL) and finally brine (150 mL). The organic fraction was dried with $MgSO_4$, and the volatiles removed under reduced pressure. The resultant solid was dissolved in toluene (200 mL), and the volatiles removed under reduced pressure. Subjecting the resultant solid to flash column chromatography (3:2 heptane:dichloromethane) gave **12** and **10**.

Yield: 12; 1.84 g, 2.52 mmol, 89% and **10**; 0.042g, 0.057 mmol, 2%

^{1}H NMR (500 MHz, CD_2Cl_2) δ 7.56 (s, 2H), 7.31 (s, 2H), 7.22 (s, 2H), 7.04 (d, J = 5.0 Hz, 1H), 5.54 (d, J = 5.0 Hz, 1H), 4.28 (t, J = 7.4, 4H), 3.71 (s, 2H), 1.89 (sxt, J = 7.5 Hz, 4H), 0.96 (t, J = 7.4 Hz, 4H).
^{13}C NMR (125 MHz, $CDCl_3$) δ 12.11, 22.55, 29.70, 29.88, 34.93, 35.39, 44.77, 50.29, 105.75, 106.32, 110.02, 114.36, 117.29, 118.56, 119.10, 132.49, 135.86, 136.03, 137.88, 147.35, 151.29.

Synthesis of **13**

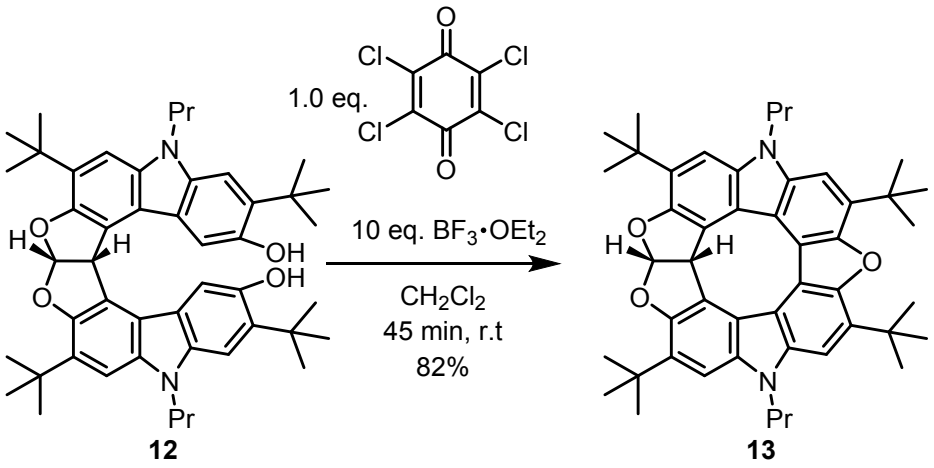

Procedure: To a round bottomed flask, equipped with a magnetic stir bar, was added **12** (210 mg, 0.288 mmol, 1.0 eq.) which was dissolved in dichloromethane (2.9 mL). To the stirred solution was added chloranil (70.8 mg, 0.288 mmol, 1.0 eq.) and $BF_3 \bullet OEt_2$ (0.253 mL, 2.88 mmol, 10 eq.), and the reaction was stirred for 45 minutes. To the completed reaction was added water (10 mL) and the suspension was extracted three times with dichloromethane (3x10 mL). The combined organic layers were dried with $MgSO_4$, and the volatiles removed under reduced pressure. The resultant solid was purified with flash column chromatography (dichloromethane:heptane) giving **13** as a solid.

Yield: 168 mg, 0.237 mmol, 82%

^{1}H-NMR (500 MHz, CD_2Cl_2) δ 7.48 (s, 2H), 7.28 (s, 2H), 7.07 (d, J = 7.8 Hz, 2H), 5.57 (d, J = 7.8 Hz, 2H), 4.48-4.35 (m, 4H), 1.95-1.88 (m, 4H), 1.78 (s, 18H), 1.57 (s, 18H), 0.99 – 0.91 (m, 6H).

^{13}C-NMR (126 MHz, CD_2Cl_2) δ 150.43, 149.91, 138.37, 136.95, 133.64, 132.15, 119.22, 118.03, 117.34, 113.29, 111.88, 105.68, 105.65, 51.78, 44.97, 35.21, 35.05, 30.64, 29.70, 22.69, 11.97.

HR-MS (MALDI-TOF): calcd. for $C_{48}H_{56}N_2O_3[M]^{\bullet+}$ is 708.4291 m/z, found 708.4278.

Synthesis of **10**

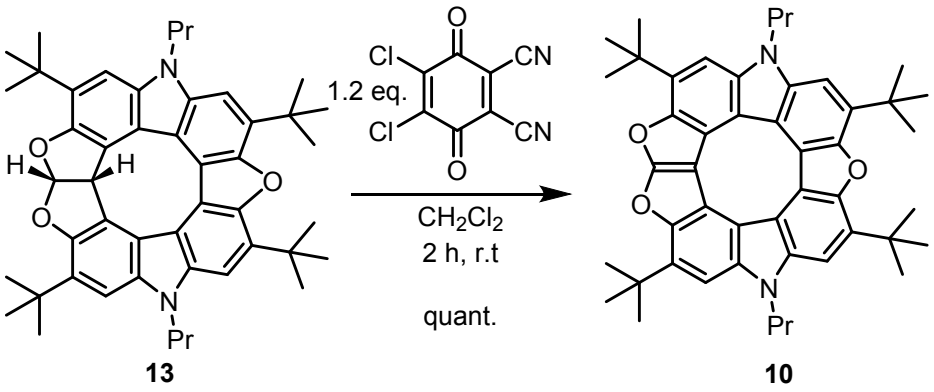

Procedure: To a flame dried round bottomed flask, wrapped in tin foil (to shield from light) and equipped with a magnetic stir bar, was added **13** (93 mg, 0.13 mmol, 1.0 eq.) which was dissolved in anhydrous dichloromethane (2.6 mL). To the stirred reaction was added DDQ (36 mg, 0.16 mmol, 1.2 eq.) and a nitrogen atmosphere was fitted. The reaction was left stirring for 2 hours, upon which 0.2 M NaOH (10 mL) was added, and the resultant suspension was extracted three times with toluene (3x10 mL). The combined organic fractions were dried with $MgSO_4$ and the volatiles removed under reduced pressure to give pure **10**.

Yield: 93 mg, 0.13 mmol, quantitative

Comment: Careful measures should be taken to avoid subjecting **10** to direct light as it is prone to decomposition, especially when handled in solution. In our hands, turning the lights of in the fumehood and lab were sufficient. A solid sample, kept shielded from light, showed no sign of decomposition after 2 months.
Aggregates was observed in NMR at concentrations above 0.02 M.

^{1}H NMR:(500 MHz, CD_2Cl_2) δ 7.93 (s, 2H), 7.51 (s, 2H), 4.70 (t, J = 7.3 Hz, 4H), 2.12 (sxt, J = 7.3 Hz, 4H), 1.89 (s, 18H), 1.81 (s, 18H), 1.12 (t, J = 7.3 Hz, 6H).

^{13}C NMR:(126 MHz, CD_2Cl_2) δ 149.81, 147.52, 137.36, 137.18, 132.89, 131.84, 118.42, 116.33, 112.52, 112.14, 106.12, 99.68, 45.08, 35.31, 35.11, 30.47, 30.28, 22.50, 12.02.

HR-MS (MALDI-TOF): calcd. for $C_{48}H_{54}N_2O_3[M]^{\bullet+}$ is 706.4134 m/z, found 706.4128.

Synthesis of **10**

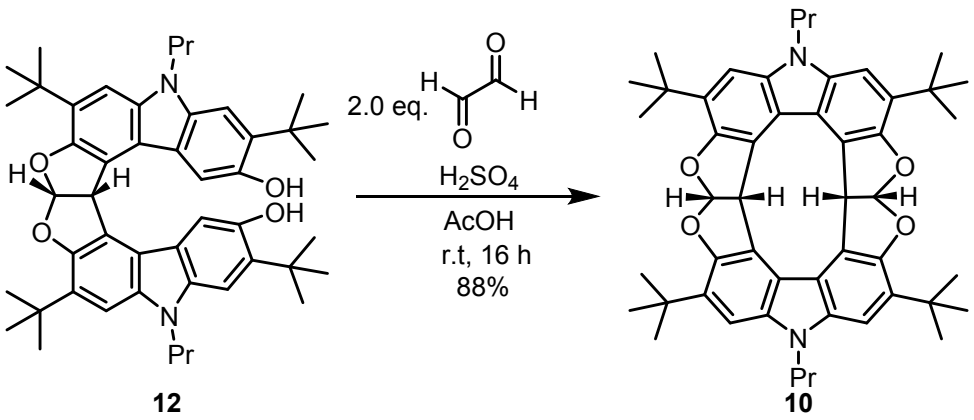

12 **10**

Procedure: To a round bottomed flask, equipped with a magnetic stir bar, was added **A** (600 mg, 0.823 mmol 1.0 eq.) along with glacial AcOH (16.5 mL) and the suspension was heated to 75 °C. Glyoxal (40wt% in H_2O, 0.189 ml, 1.65 mmol, 2.00 eq.) along with concentrated H_2SO_4 (0.165 ml, 3.09 mmol, 3.75 eq.) was added and the reaction was stirred for 16 hours. The completed reaction was cooled to room temperature and water (100 mL) was added. The resultant suspension was filtered, and the filtrate collected. Subjection to flash column chromatography (4:1 dichloromethane:heptane) provided **D** as a yellow solid.

Yield: 0.546 g, 0.727 mmol, 88%

^{1}H-NMR (500 MHz, CD_2Cl_2) δ 7.17 (d, J = 6.5, 2H), 7.08 (s, 4H), 6.20 (d, J = 6.5 Hz, 2H), 4.13z (t, J = 7.1 Hz, 4H), 1.81-1.72 (m, 4H), 1.49-1.45 (m, 36H), 0.90 (t, J = 7.5 Hz, 6H).

^{13}C-NMR (126 MHz, CD_2Cl_2) δ 150.61, 138.20, 132.45, 119.38, 115.83, 110.54, 106.02, 52.81, 44.98, 35.02, 29.50, 22.50, 11.91.

HR-MS (MALDI-TOF): calcd. for $C_{50}H_{58}N_2O_4[M]^{\bullet+}$ is 750.4397 m/z, found 750.4385.

6. NMR Spectra

^{1}H-NMR of **12** in CD_2Cl_2

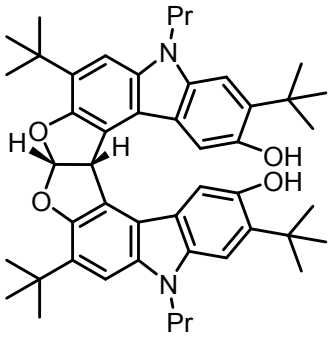

12

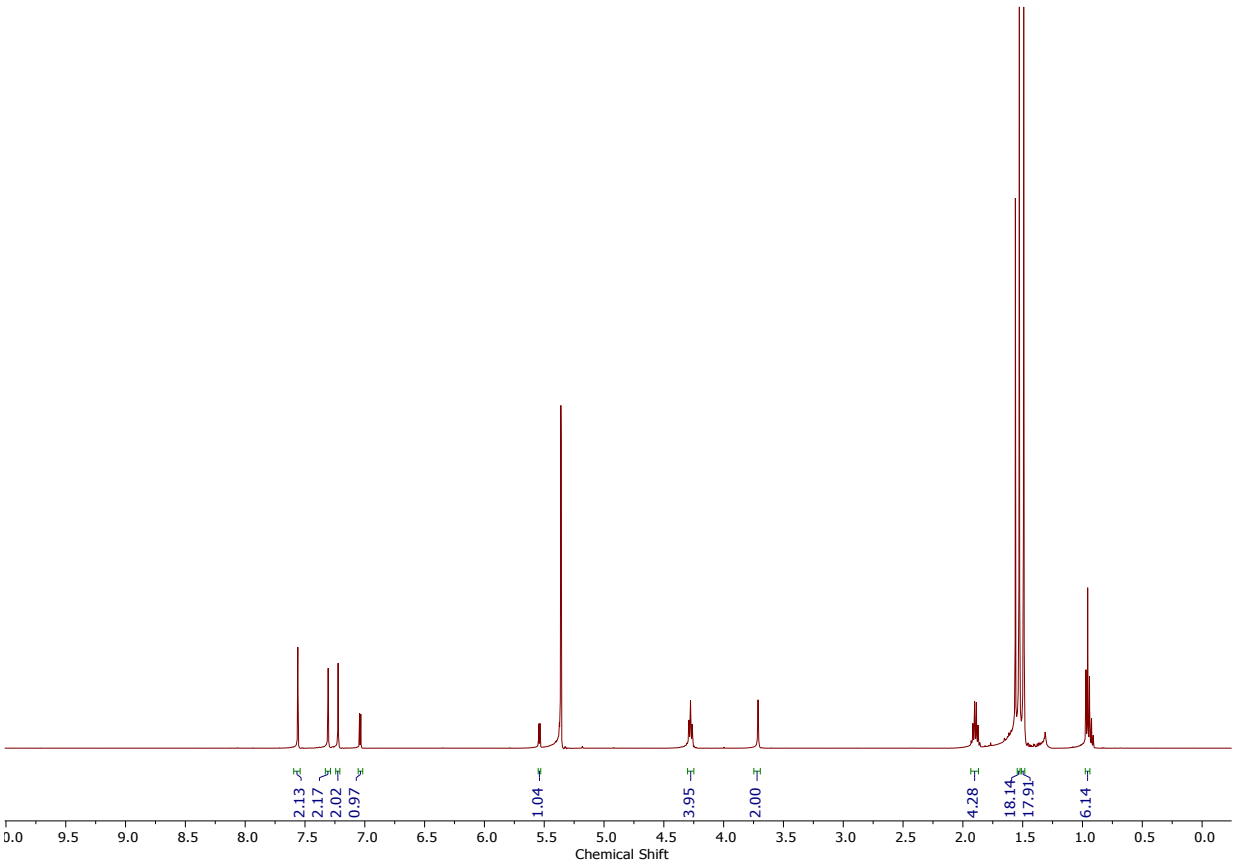

^{13}C-NMR of **12** in $CDCl_3$

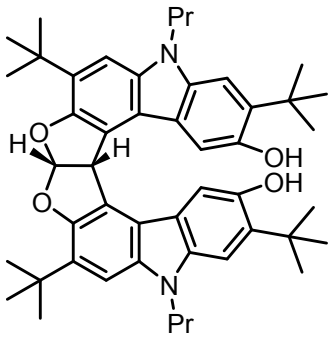

12

J0002.11.fid
Email= pittel@kiku.dk
stekorped-12
C13CPD32 CDCl3 /opt/topspin/data bnmr1 18

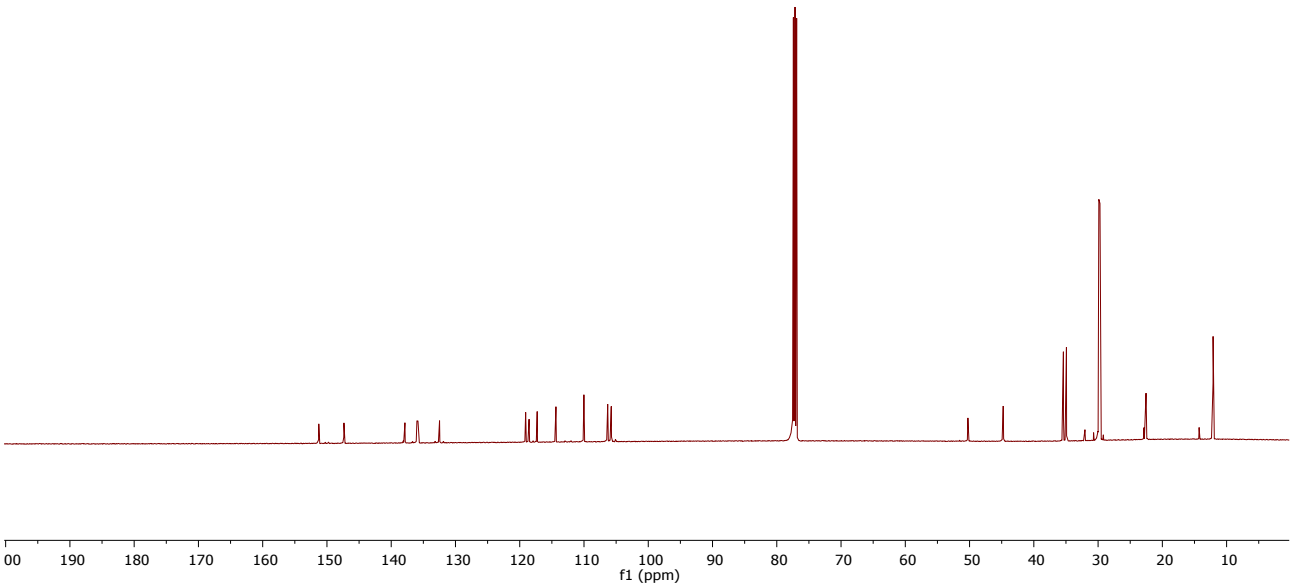

^{1}H-NMR of **13** in CD_2Cl_2

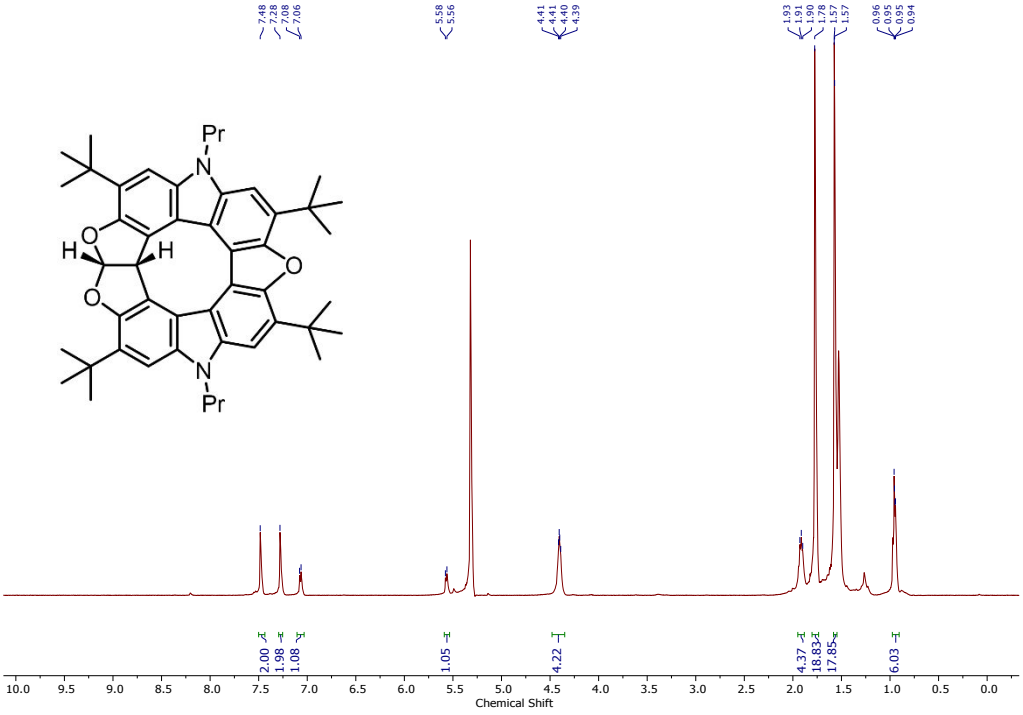

^{13}C-NMR of **B** in CD_2Cl_2

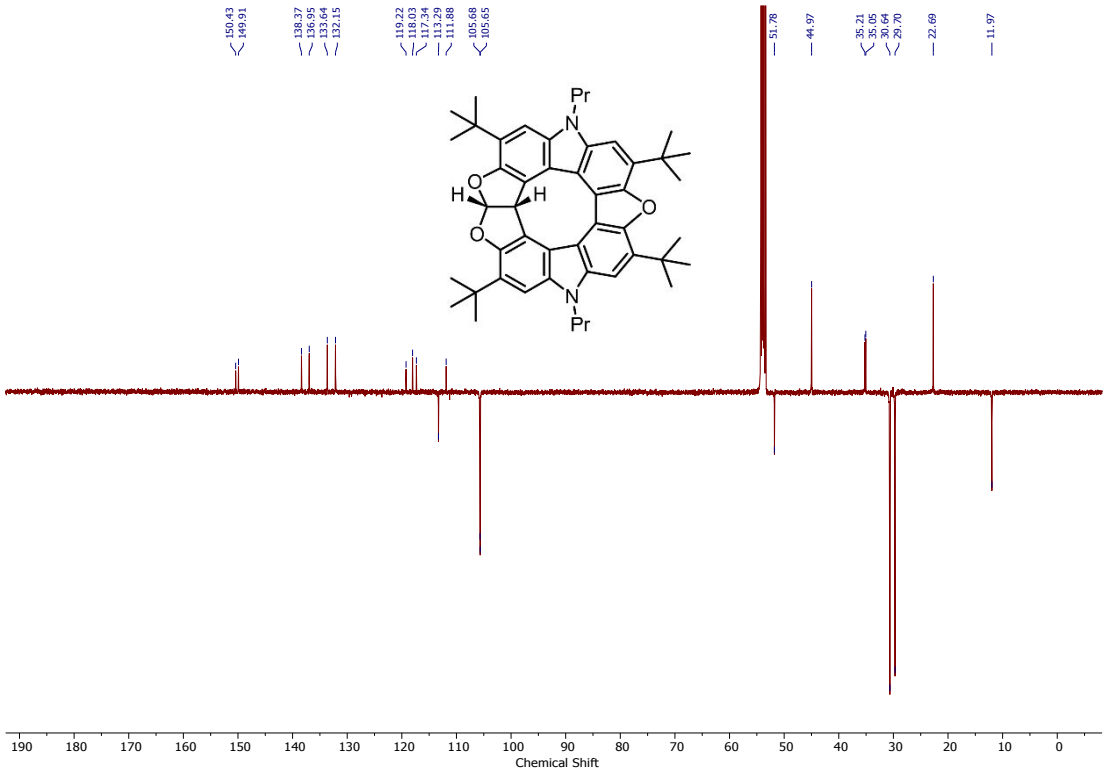

^{1}H-NMR of **9** in CD_2Cl_2

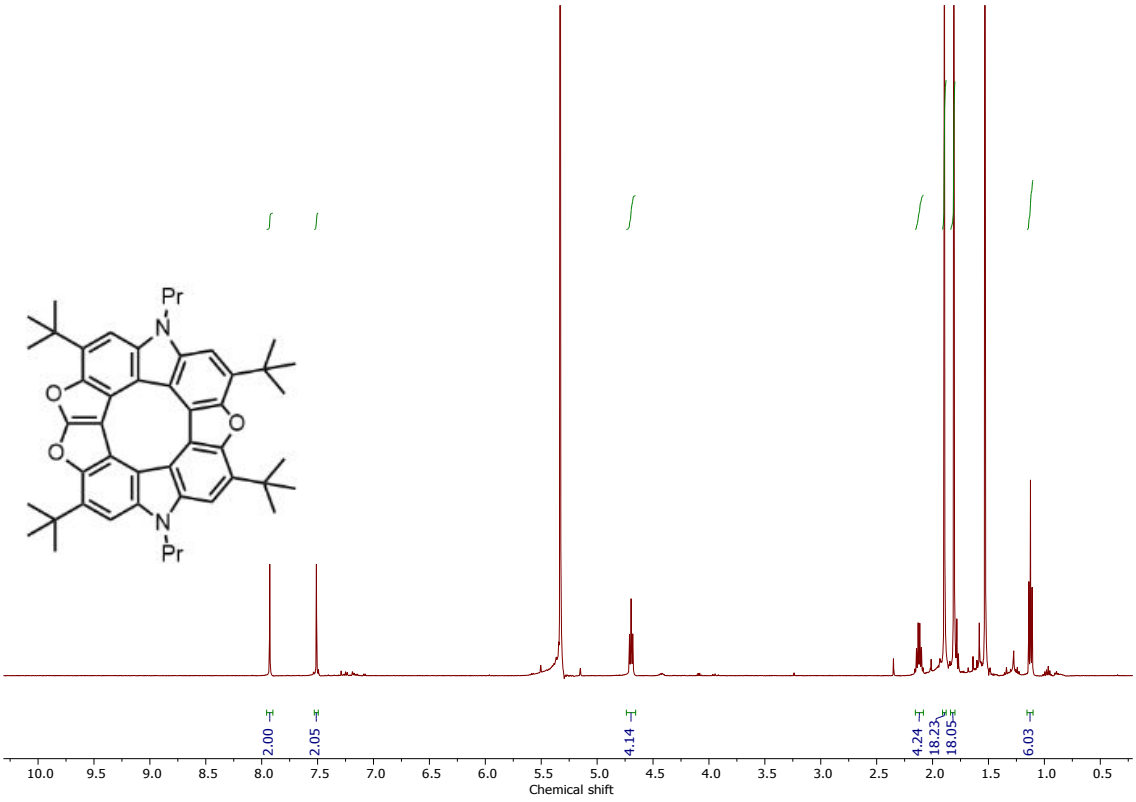

^{13}C-NMR of **9** in CD_2Cl_2

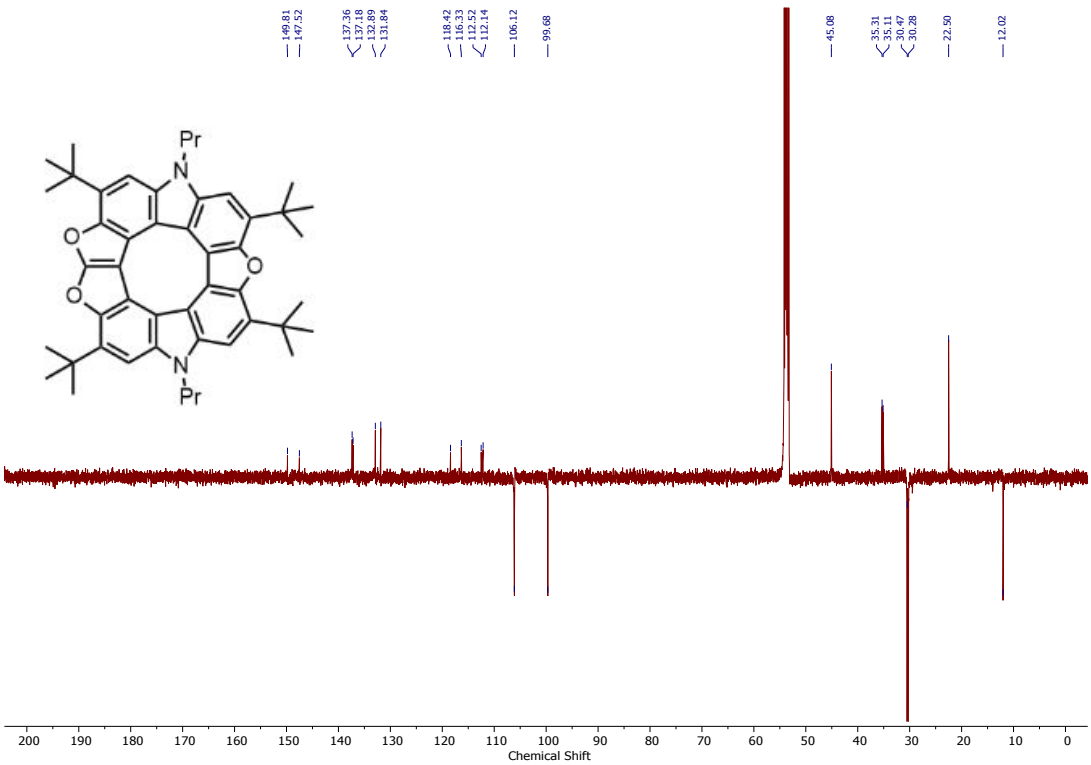

^{1}H-NMR of **10** in CD_2Cl_2

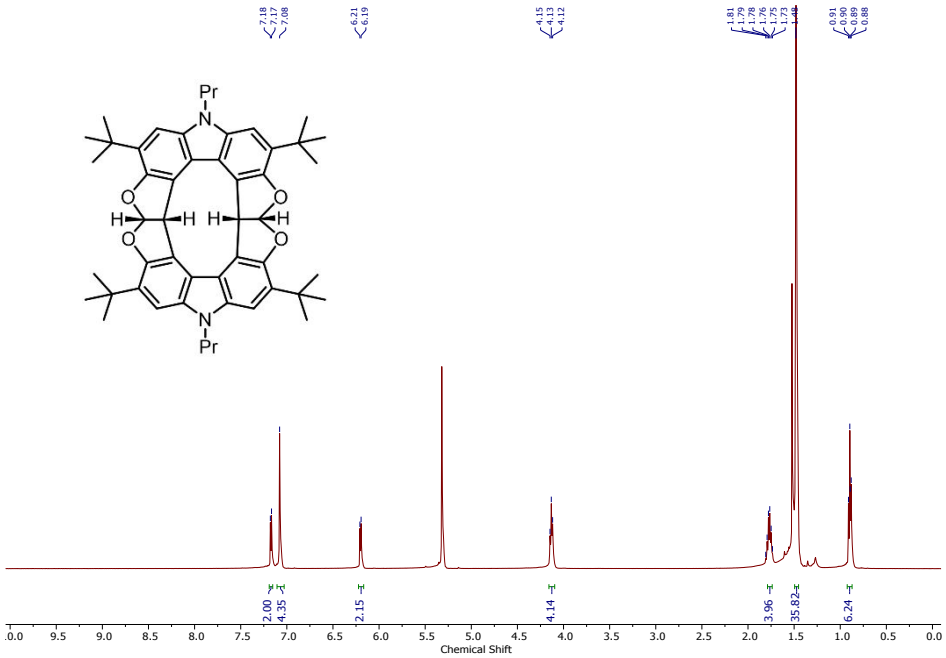

^{13}C-NMR of **10** in CD_2Cl_2

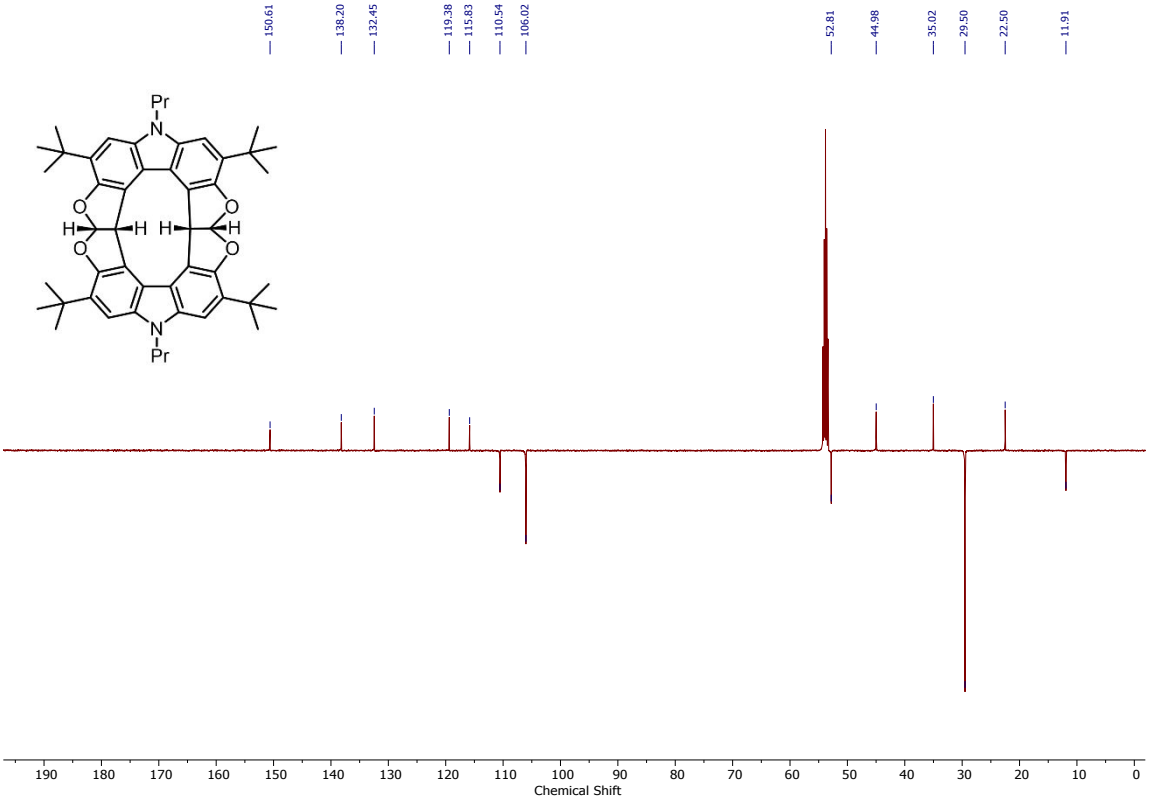

7. References

1. A. D. Becke, Density-functional thermochemistry. III. The role of exact exchange, *J. Chem. Phys.* 1993, **98**, 5648–5652.
2. C. Lee, C. Hill and N. Carolina, Electronic structure calculations on workstation computers: The program system turbomole, *Chem. Phys. Lett.* 1989, **162**, 165–169.
3. R. Ditchfield, W. J. Hehre and J. A. Pople, Self-consistent molecular orbital methods. XII. Further extensions of Gaussian-type basis sets for use in molecular orbital studies of organic molecules, *J. Chem. Phys.* 1971, **54**, 724–728.
4. J. Tomasi, B. Mennucci and R. Cammi, Quantum mechanical continuum solvation models, *Chem. Rev.*, 2005, **105**, 2999–3093.
5. S. I. Gorelsky, *SWizard program*, University of Ottawa, Ottawa, 2010. http://www.sg-chem.net.
6. Z. Chen, C. S. Wannere, C. Corminboeuf, R. Puchta and P. von Ragué Schleyer, Nucleus-independent chemical shift (NICS) as an aromaticity criterion, *Chem. Rev.* 2005, **105**, 3842–3888.
7. A. D. McLean and G. S. Chandler, Contracted Gaussian basis sets for molecular calculations. I. Second row atoms, Z=11-18, *J. Chem. Phys.* 1980, **72**, 5639–5648.
8. T. Clark, J. Chandrasekhar and G. W. Spitznagel, The impact of p-orbital on optimization of $ReH_7(PMe_3)_2$ compound, *J. Comput. Chem.* 1983, **4**, 294–301.
9. K. Wolinski, J. F. Hinton and P. Pulay, Efficient implementation of the gauge-independent atomic orbital method for NMR chemical shift calculations, *J. Am. Chem. Soc.* 1990, **112**, 8251–8260.
10. G. V. Baryshnikov, B. F. Minaev, M. Pittelkow, C. B. Nielsen and R. Salcedo, Nucleus-independent chemical shift criterion for aromaticity in π-extended tetraoxa[8]circulenes, *J. Mol. Model.* 2013, **19**, 847–850.
11. G. V. Baryshnikov, N. N. Karaush and B. F. Minaev, The electronic structure of heteroannelated cyclooctatetraenes and their UV-Vis absorption spectra, *Chem. Heterocycl. Comp.* 2014, **50**, 349–363.
12. S. F. Nelsen and F. Blomgren, Estimation of electron transfer parameters from AM1 calculations, *J. Org. Chem.* 2001, **66**, 6551–6559.
13. S. F. Nelsen, D. A. Trieber Ii, R. F. Ismagilov and Y. Teki, Solvent effects on charge transfer bands of nitrogen centered intervalence compounds, *J. Am. Chem. Soc.* 2001, **123**, 5684–5694.
14. M. Malagoli and J. L. Bredas, Density functional theory study of the geometric structure and energetics of triphenylamine-based hole-transporting molecules, *Chem. Phys. Lett.* 2000, **327**, 13–17.
15. K. Sakanoue, M. Motoda, M. Sugimoto and S. Sakaki, A molecular orbital study on the hole transport property of oranic amine compounds, *J. Phys. Chem. A* 1999, **103**, 5551–5556.
16. X. Y. Li, J. Tong and F. C. He, Observation of all-trans-β-carotene wavepacket motion on the electronic ground and excited dark state using degenerate four-wave (DFWM) and pump-DFWM, *Chem. Phys.* 2000, **260**, 283–294.
17. R. A. Marcus and N. Sutin, Electron transfer in chemistry and biology, *Biochim. Biophys. Acta* 1985, **811**, 265–322.
18. R. A. Marcus, Electron transfer reactions in chemistry. Theory and experiments, *Rev. Mod. Phys.* 1993, **65**, 599–610.
19. R. A. Marcus, On the theory of oxidation-reduction reactions involving electron transfer, *J. Chem. Phys.* 1956, **24**, 966–978.
20. N. S. Hush, Adiabatic rate processes at electrodes. I. Energy-charge relationships, *J. Chem. Phys.* 1958, **28**, 962–972.

21. N. S. Hush, Adiabatic theory of outer sphere electron-transfer reactions in solution, *Trans. Faraday Soc.* 1961, **57**, 577–590.
22. A. Datta, S. Mohakud and S. K. Pati, Electron and hole mobilities in polymorphs of benzene and naphthalene: role of intermolecular interactions, *J. Chem. Phys.* 2007, **126**, 144710–144716.
23. A. Datta, S. Mohakud and S. K. Pati, Comparing the electron and hole mobilities in the α and β phases of perylene: role of π-stacking, *J. Mater. Chem.* 2007, **17**, 1933–1938.
24. V. Mohan and A. Datta, Structure and electronic properties of Si-substituted benzenes and their transition-metal complexes, *J. Phys. Chem. Lett.* 2010, **1**, 136–146.
25. S. Mohakud and S. K. Pati, Large carrier mobilities in octathio[8]circulene crystals: a theoretical study, *J. Mater. Chem.* 2009, **19**, 4356–4361.
26. F. Wang and T. Ziegler, A simplified relativistic time-dependent density-functional theory formalism for the calculations of excitation energies including spin-orbit coupling effects, *J. Chem. Phys.* 2005, **123**, 154102–154112.
27. E. Van Lenthe and E. J. Baerends, Optimized Slater-type basis sets for the elements 1-118, *J. Comput. Chem.* 2003, **24**, 1142–1156.
28. C. C. Pyeand and Tom Ziegler, An implementation of the conductor-like screening model of solvation within the Amsterdam density functional package, *Theor. Chem. Acc.*, 1999, **101**, 396–408.
29. P. K. Samanta, D. Kim, V. Coropceanu and J.-L. Bredas, Up-conversion intersystem crossing rates in organic emitters for thermally activated delayed fluorescence: impact of the nature of singlet vs triplet excited states, *J. Am. Chem. Soc.* 2017, **139**, 4042–4051.
30. E. van Lenthe, J. G. Snijders and E. J. Baerends, The zero-order regular approximation for relativistic effects: the effect of spin-orbit coupling in closed shell molecules, *J. Chem. Phys.* 1996, **105**, 6505–6516.
31. E. van Lenthe, R. van Leeuwen, E. J. Baerends and J. G. Snijders, Relativistic regular two-component Hamiltonians, *Int. J. Quant. Chem.* 1996, **57**, 281–293.
32. K. Mori,T. P. M. Goumans,E. van Lenthe and F. Wang, Predicting phosphorescent lifetimes and zero-field splitting of organometallic complexes with time-dependent density functional theory including spin-orbit coupling, *Phys. Chem. Chem. Phys.* 2014,**16**,14523–14530.
33. G. Baryshnikov, B. Minaev and H. Ågren, Theory and calculation of the phosphorescence phenomenon, *Chem. Rev.* 2017, **117**, 6500−6537.
34. V. G. Plotnikov, Regularities of the processes of radiationless conversion in polyatomic molecules, *Int. J. Quant. Chem.* 1979, **16**, 527–541.
35. G. V. Baryshnikov, R. R. Valiev, N. N. Karaush, V. A. Minaeva, A. N. Sinelnikov, S. K. Pedersen, M. Pittelkow, B. F. Minaev and Hans Ågren, Benzoannelated aza-, oxa-, and azaoxa[8]circulenes as promising blue organic emitters, *Phys. Chem. Chem. Phys.* 2016, **18**, 28040–28051.
36. R. R. Valiev,V. N. Cherepanov,V.Ya. Artyukhov and D. Sundholm, Computational studies of photophysical properties of porphin, tetraphenylporphyrin and tetrabenzoporphyrin, *Phys. Chem. Chem. Phys.* 2012,**14**, 11508–11517.
37. V. Ya. Artyukhov, T. N. Kopylova, L. G. Samsonova, N. I. Selivanov, V. G. Plotnikov, V. A. Sazhnikov, A. A. Khlebunov, G. V. Mayer and M. V. Alfimov, A combined theoretical and experimental study on molecular photonics, *Russ. Phys. J.*, 2008, **51**, 1097–1111.
38. R. R. Valiev, A. N. Sinelnikov, Y. V. Aksenova, R. T. Kuznetsova, M. B. Berezin, A. S. Semeikin, and V. N. Cherepanov, The computational and experimental investigations of photophysical and spectroscopic properties of BF_2 dipyrromethene complexes, *Spectrochim. Acta A* 2014, **117**, 323–329.
39. G. teVelde, F. M. Bickelhaupt, E. J. Baerends, C. Fonseca Guerra, S. J. A. van Gisbergen, J. G. Snijders and T. Ziegler, Chemistry with ADF, *J. Comput. Chem.* 2001, **22**, 931–967.
40. M. J. Frisch, G. W. Trucks, H. B. Schlegel, G. E. Scuseria, M. A. Robb, J. R. Cheeseman, G. Scalmani, V. Barone, B. Mennucci, G. A. Petersson, H. Nakatsuji, M. Caricato, X. Li, H. P. Hratchian, A. F. Izmaylov,

J. Bloino, G. Zheng,J. L. Sonnenberg, M. Hada, M. Ehara, K. Toyota, R. Fukuda, J. Hasegawa, M. Ishida, T. Nakajima, Y. Honda, O. Kitao, H. Nakai, T. Vreven, J. A. Montgomery, Jr., J. E. Peralta, F. Ogliaro, M. Bearpark, J. J. Heyd, E. Brothers, K. N. Kudin, V. N. Staroverov, R. Kobayashi, J. Normand, K. Raghavachari, A. Rendell, J. C. Burant, S. S. Iyengar, J. Tomasi, M. Cossi, N. Rega, J. M. Millam, M. Klene, J. E. Knox, J. B. Cross,V. Bakken, C. Adamo, J. Jaramillo, R. Gomperts, R. E. Stratmann, O. Yazyev, A. J. Austin, R. Cammi, C. Pomelli, J. W. Ochterski, R. L. Martin, K. Morokuma, V. G. Zakrzewski, G. A. Voth, P. Salvador, J. J. Dannenberg, S. Dapprich, A. D. Daniels, O.Ë. Farkas, J. B. Foresman, J. V. Ortiz, J. Cioslowski and D. J. Fox, *Gaussian 16, Rev. A. 03*, Gaussian, Inc., Wallingford, CT, 2016.